1974

Cross sections for photoionization of the 6²P-fine structure levels of cesium

John Daniel Jones

Department: Physics

CROSS SECTIONS FOR PHOTOIONIZATION OF THE 6^2P-FINE STRUCTURE LEVELS OF CESIUM

by

JOHN DANIEL JONES, 1948 -

A DISSERTATION

Presented to the Faculty of the Graduate School of the

UNIVERSITY OF MISSOURI - ROLLA

In Partial Fulfillment of the

Requirements for the Degree

DOCTOR OF PHILOSOPHY

in

PHYSICS

1974

Karl J. Nygaard
Advisor

William R. Inman

Tom Dolan

David L. Scheaver

Jerry L. Peacher

ABSTRACT

The cross sections for photoionization of excited cesium from the $6^2P_{3/2}$- and $6^2P_{1/2}$-fine structure levels have been measured using a triple crossed-beam apparatus. Two photon beams, one for excitation and one for ionization, impinge upon an atomic beam and produce ions at the point of intersection. The relative cross section is determined from a knowledge of the ion count rate and the relative photon flux of the ionization light. The results are normalized to available theoretical calculations and compared with recombination measurements in cesium plasmas. The present cross sections are found to decrease with decreasing wavelength more rapidly than predicted by theory, but are in excellent agreement with previous experimental studies of the combined 6^2P-states.

ACKNOWLEDGEMENTS

I would like to thank my advisor, Dr. Kaare J. Nygaard. His cooperation, advice, and support made the successful completion of this research effort possible. I would like to express my appreciation to Dr. Robert E. Hebner, Jr. for his previous work in this field and especially for his personal support in the initial stages of this program. Beaufort Lancaster has made innumerable day-to-day contributions for which I am grateful. Also, I would like to thank my advisory committee whose time and efforts have been greatly appreciated. For the financial support that enabled me to carry out this program, I would like to thank the Department of Physics, University of Missouri - Rolla and the Office of Naval Research. Finally, I would like to thank my wife, Carol, whose contributions are immeasurable.

TABLE OF CONTENTS

LIST OF ILLUSTRATIONS

I. INTRODUCTION

The present study is designed to determine the photoionization cross section of cesium from the first excited state. Cesium is used extensively in many plasma devices such as thermionic energy converters, ion and plasma propulsion engines, MHD generators, and lasers. In many of these devices a high density of excited states can occur. Since the cross section for photoionization from the first excited state is reported to be two orders of magnitude larger than from the ground state[1-4], this process could become an important ionization mechanism in these devices. Although there is general agreement between experiment and theory as to the absolute value of the photoionization cross section at threshold, there is disagreement over the variation of this cross section with wavelength, and some question as to the reliability of the earlier experiments[5]. Another reason to perform this study is to establish a general procedure for determining two-step photoionization cross sections since this process is being used in such commercial applications as isotope separation[6]. The photoionization cross sections for the fine structure levels of cesium, $6^2P_{3/2}$ and $6^2P_{1/2}$, have been determined in an attempt to clarify the present controversy and to establish experimental techniques for determining similar cross sections.

The simplified term diagram shown in Fig. 1 gives energy spacings of the 6^2P-states and the ionization

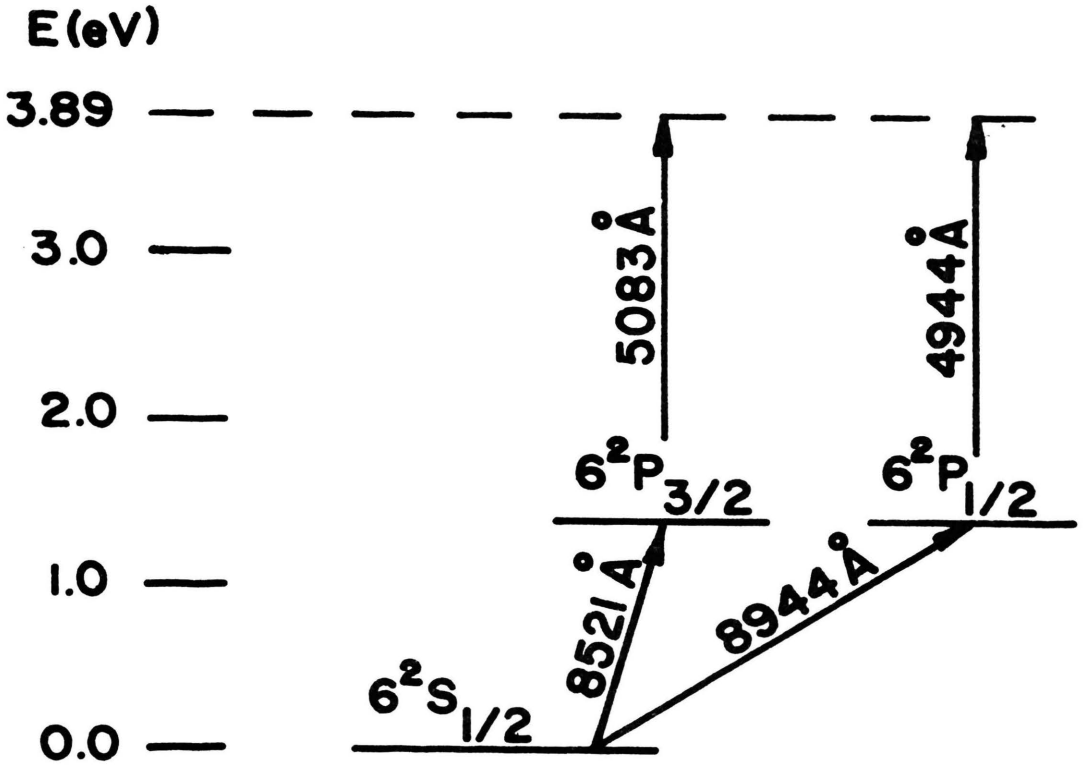

Fig. 1. Partial energy-level diagram for cesium. The "onset" wavelengths for photoionization from the fine structure states are included.

threshold (3.89 eV) relative to the ground state. The wavelengths of the excitation and ionization transitions are also indicated. The specific reaction to be studied proceeds in two steps. First, the ground state atoms are excited according to the process

$$Cs(6^2S_{1/2}) + h\nu_o \rightarrow Cs^*(6^2P_{3/2,1/2}), \qquad (1.1)$$

where $h\nu_o$ represents the resonance energy of the indicated transition. It is possible to provide this energy in a variety of forms. In this study photoexcitation is chosen because the wavelengths necessary for these transitions, 8521 Å for excitation to the $6^2P_{3/2}$-state and 8944 Å for excitation to the $6^2P_{1/2}$-state, are separated by 423 Å and are easily selected with the aid of interference filters. This allows either the $6^2P_{3/2}$- or $6^2P_{1/2}$-state to be selectively excited for study.

The second stage of the reaction is

$$Cs^*(6^2P_{3/2,1/2}) + h\nu \rightarrow Cs^+ + e^-, \qquad (1.2)$$

where $h\nu$ is the photon energy. This process represents a bound-free transition, as opposed to the bound-bound transition in Eq. (1.1). Continuous absorption will take place for photon energies greater than threshold, corresponding to wavelengths of 5083 and 4944 Å for the $6^2P_{3/2}$- and $6^2P_{1/2}$-states, respectively.

In the past photoionization cross sections for cesium have been determined in several different ways[7-8]. One of these methods is to determine the transmission of a uv light source through a column of cesium vapor. In this approach[9] the spectrum of a uv lamp is recorded on a photographic plate before and after cesium vapor is introduced into the optical path. The photoionization cross section is found from

$$\ell n \frac{I(\lambda)}{I_o(\lambda)} = - \sigma_a(\lambda)\, n_o x, \qquad (1.3)$$

where $I_o(\lambda)$ and $I(\lambda)$ are the incident and transmitted photon fluxes, respectively, n_o is the number density of cesium atoms, x is the path length of the light through the vapor, and $\sigma_a(\lambda)$ is the absorption cross section. The main problem associated with this approach is that the path length, x, must be long to obtain appreciable attenuation of the incident photon beam. Furthermore, it is difficult to determine the density of cesium atoms over the path length and to ensure its uniformity.

Other methods involve the determination of the recombination cross section which can be related to the photoionization cross section through detailed balancing. One approach is to measure the rate of loss of electrons in a cesium plasma[3]. Another technique is to observe the recombination spectra of a cesium plasma[4]. These methods are applicable to the ground state and excited states and the

results of these two methods for the combined 6^2P-states of cesium are shown in Fig. 2. The major difficulty associated with recombination experiments is to accurately determine the energy distribution of the electrons involved in the recombination process.

The present experiment is designed to avoid many of the problems associated with the previous work and represents the first successful attempt to directly measure the photoionization cross section from the fine structure levels of the first excited state of cesium. The triple crossed-beam apparatus used in this experiment consists of an atomic beam crossed by two photon beams, one for excitation and one for ionization. The three beams intersect within a small volume and produce ions, which are counted. The cross section is then proportional to the count rate.

The absolute cross section for photoionization from the excited state as a function of the incident ionization wavelength, λ, can be written as

$$\sigma_{abs}(\lambda) = \left[\frac{4\pi^2\theta c\tau\alpha_c^2 r_o f V}{\Delta\nu}\right]^{-1} \frac{N^+(\lambda)}{j_1(\lambda_o)j_2(\lambda)n_o} \quad (1.4)$$

where r_o is the first Bohr radius, c is the speed of light, τ is the lifetime of the excited state, f is the oscillator strength of the transition from the ground state to the excited state, θ is the overall efficiency of the ion extraction and counting system, V is the interaction volume, n_o is the atomic beam density, α_c is the fine structure

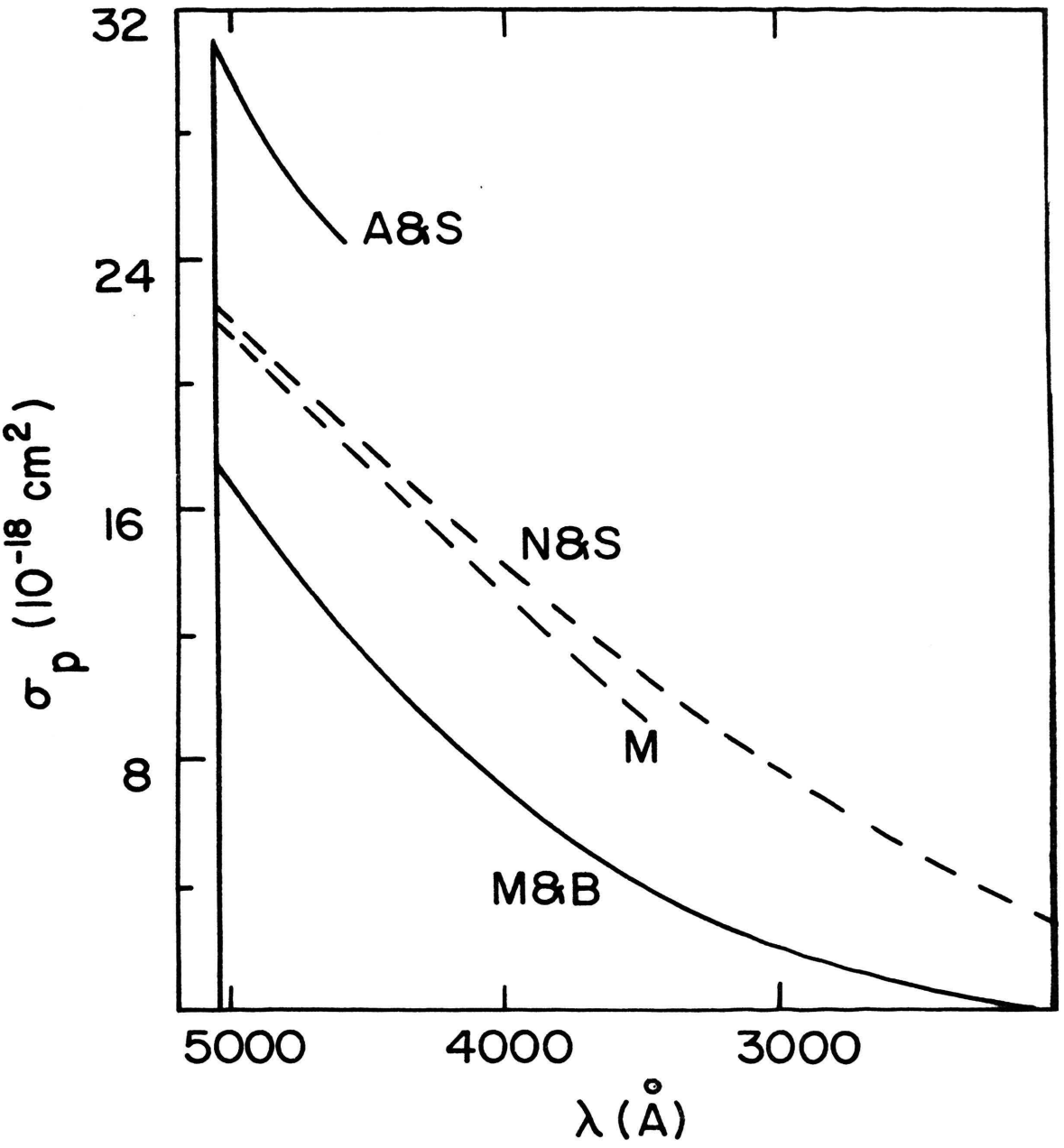

Fig. 2. Photoionization cross section from the combined 6^2P-states of cesium. The experimental curves are from measurements by Mohler and Boeckner[3] (M&B) and Agnew and Summers[4], (A & S). Theoretical curves represent a calculation using the quantum defect method by Moskvin[16] (M), and the adjusted quantum defect method of Norcross and Stone[1] (N & S).

constant, $\Delta\nu$ represents the frequency interval associated with $j_1(\lambda_o)$, $N^+(\lambda)$ is the observed net count rate, and $j_1(\lambda_o)$ and $j_2(\lambda)$ represent the photon fluxes of the excitation and the ionization radiation, respectively. The relative photoionization cross section as used in this work is

$$\sigma(\lambda) \propto \frac{N^+(\lambda)}{j_2(\lambda)} , \tag{1.5}$$

where it is assumed that the remaining quantities in Eq. (1.4) do not change for the various ionization wavelengths.

Advantages of this technique are numerous. Since attenuation measurements are not used, it is not necessary to measure the ratio of the incident to transmitted photon flux. Also, it is not necessary to determine the energy distribution of the electrons as is the case for recombination measurements. It is convenient to use an atomic beam instead of a vapor cell because of the chemical reactivity of cesium. In general, the small angular spread and uniform density in a beam are also advantageous. Furthermore, broadening of the absorption line due to collisions is minimized leaving only Doppler broadening to be considered. Another advantage of this design is the ability to allow for unwanted ionization processes, such as electron impact ionization and photoionization of ground state atoms and dimers (Cs_2), by modulating one of the three beams. Similar

crossed-beam techniques have been employed with a great deal of success[10].

The remainder of this paper is devoted to a more detailed development of this problem. A review of the various theoretical approaches to photoionization is given in Sec. II. In Sec. III a thorough description of the apparatus is given. The various excitation and ionization processes are discussed in Sec. IV. Finally, the results are presented and discussed in Sec. V.

II. THEORY

Several attempts have been made to calculate atomic photoionization cross sections, with various degrees of success[11]. For the most part these calculations have been limited to the photoionization of atoms from the ground state. At the present time, however, there exists two theories dealing specifically with photoionization of cesium from the first excited state and each will be considered later in this section.

As early as 1923, Kramers[12] introduced an expression for the photoionization cross section. His work was based on classical electrodynamic theory and the Bohr model of the atom. This formulation met with some success when applied to hydrogen and the lighter hydrogen-like ions. However, when it was applied to the heavier ions there was considerable discrepancy between theory and available experimental results.

From a quantum mechanical consideration, the photoionization cross section is proportional to the square of the transition matrix,

$$T_{n\ell,n'\ell'} = |\langle n\ell|r|n'\ell'\rangle|, \qquad (2.1)$$

where the transition is from the bound state characterized by $n\ell$ to the free state $n'\ell'$. The problem then is to find the proper wave functions and perform the integrations in Eq. (2.1).

Some noteworthy approaches to this problem are the central field approximation, consideration of the wave function with exchange, core polarization, the dipole formulation, the random phase approximation, and the unrelaxed core method. Each of these methods have met with some success when applied to a particular atomic system, however, at this time there seems to be no general rule to predict which approach gives the most reliable results when applied to another system.

More recent calculations involving the lighter alkali atoms include calculations involving independent particle models[5]. Also a model potential calculation for lithium has been completed[13].

As has been previously stated, the foregoing theories are concerned for the most part with photoionization of atoms from the ground state. Each, however, may be applied to the problem of excited state photoionization, but an additional difficulty arises in the calculation of the proper wave functions.

At this point two theories will be considered in more detail. One of these is a method introduced by Norcross and Stone[1] referred to as the adjusted quantum defect method (AQDM) and based on the quantum defect method (QDM). The QDM was introduced in connection with photoionization by Burgess and Seaton[14] and it will be necessary to first consider this approach. The other theory to be considered is a model potential calculation by Weisheit[2].

A. Quantum Defect Method

The QDM is designed for a single electron moving in a central field and gives the matrix elements for the bound-bound and the bound-free transitions if the energy levels of the atomic system are known. The radial wave function for the valence electron of a neutral cesium atom satisfies

$$\left[\frac{d^2}{dr^2} - \frac{\ell(\ell+1)}{r^2} - V(r) + \varepsilon\right] y(\varepsilon,\ell,r) = 0, \qquad (2.2)$$

where r is the radius in atomic units, and V(r) and ε are the potential and energy in Rydbergs. $y(\varepsilon,\ell,r)$ represents the radial wavefunction. It is assumed for large r,

$$V(r) = -2/r, \qquad (2.3)$$

and for small r, the potential is unknown.

For continuum states ($\varepsilon > 0$), let

$$\varepsilon = 1/\gamma^2, \qquad (2.4)$$

and

$$y(\gamma,\ell,r) = F_{n\ell}(r), \qquad (2.5)$$

where $F_{n\ell}(r)$ represents the normalized free state solutions,

using delta function normalization. Also $F_{n\ell}(r)$ is required to have an asymptotic form, differing only in phase from the solution for a pure Coulomb field.

The desired transition integrals for the bound-free transitions are (with primes indicating upper levels)

$$\langle \eta\ell | r | \gamma'\ell' \rangle = \int_0^\infty P_{n\ell}(r) r F_{\gamma',\ell'}(r)\, dr, \qquad (2.6)$$

where η is the effective quantum number of the bound state ($\varepsilon < 0$). The quantum defect is defined as

$$\mu_\ell(\eta) = n - \eta, \qquad (2.7)$$

where n is the usual integral quantum number.

For large r, Eq. (2.2) can be written

$$\left[\frac{d^2}{dr^2} - \frac{\ell(\ell+1)}{r^2} + \frac{2}{r} - \frac{1}{\kappa^2} \right] y(\kappa,\ell,r) = 0 \qquad (2.8)$$

where $\kappa = \eta$ for $\varepsilon < 0$ and $\kappa = i\gamma$ for $\varepsilon > 0$. The desired radial wave functions are given by linear combinations of solutions of Eq. (2.8) with constants determined from the normalization procedure. For small r, these solutions have values dependent on two parameters which must be chosen. Proper choice of these parameters yield

$$|\langle \eta\ell | r | \gamma'\ell' \rangle|^2 = g^2(\eta\ell, \gamma'\ell'), \qquad (2.9)$$

where

$$g(\eta\ell,\kappa'\ell') = \eta^2 L^{-1/2}(\eta,\ell)\ G(\eta\ell,\kappa'\ell')$$
$$\times \cos\pi(\eta + \mu_{\ell'}(\kappa') + \chi(\eta\ell,\kappa'\ell')) \qquad (2.10)$$

and

$$L(\eta,\ell) = 1 + \frac{2}{\eta^3}\ \frac{\partial \mu_\ell(\eta)}{\partial \varepsilon}\ . \qquad (2.11)$$

$L(\eta,\ell)$ is approximately equal to one for cesium. G and χ are tabulated functions[14].

B. Adjusted Quantum Defect Method

The major problem associated with the QDM is that in the foregoing integrals the sensitivity to small radius behavior is dependent upon the transition involved. Since the misrepresentation of the small radius behavior affects the relative phase of the wavefunction more than the amplitude, Norcross and Stone[1] adjusted this procedure such that for large κ', the integrals depend only on η,ℓ,ℓ', and the phase. This was done by introducing a variable parameter $\gamma_{\ell\ell'}(\eta)$, in the argument of the cosine term, $\cos\pi[\eta+\mu_{\ell'}(\kappa) + \chi(\eta\ell,\kappa'\ell') + \gamma_{\ell\ell'}(\eta)]$. The parameter, $\gamma_{\ell\ell'}(\eta)$, was adjusted to the value which would bring the QDM oscillator strengths into best agreement with the oscillator strengths calculated by Stone[15], which were chosen because of their demonstrated validity.

Using this method the cross section for recombination to the 6P-state for temperatures from 1000 to 3400 ^{o}K was calculated. The photoionization cross section σ, can be determined from the recombination cross section[1], $\sigma_R(v)$ from

$$\sigma = \frac{(mv)^2}{(h\nu/c)^2 2(2\ell+1)} \sigma_R(v) \left[1 - \exp(\frac{-h\nu}{kT})\right] , \quad (2.12)$$

where T represents the temperature of the recombination plasma.

The results of this calculation are shown in Fig. 2. For comparison, a calculation by Moskvin[16] using the QDM is shown along with the experimental results of Mohler and Boeckner[3] and Agnew and Summers[4].

C. Model Potential Calculation

This calculation, which is due to Weisheit[2], describes a single electron moving in a central field and includes spin orbit perturbation of the valence electron orbitals and the polarization interaction between the valence and the core electrons. Since the valence electron of an alkali atom lies well outside the core, exchange between valence and core was neglected. For this same reason the valence and core electron motions were assumed separable[18], giving an atomic wave function of the form,

$$\Psi_a(\bar{r}_j,\bar{r}) = X_o(\bar{r}_j|\bar{r})\psi_a(\bar{r}) , \quad (2.13)$$

where X_o is the ground state core wavefunction, ψ_a is the valence-electron orbital, and $\bar{r}_j$ and $\bar{r}$ represent the location of the core electrons and the valence electron, respectively.

The eigenvalue equation for ψ_a is

$$\left[-\frac{1}{2}\bar{\nabla}_r^2 + V(\bar{r}) - \varepsilon_a \right] \psi_a(\bar{r}) = 0, \tag{2.14}$$

where

$$V(\bar{r}) = -Zr^{-1} + \langle X_o | \{-(1/2)\bar{\nabla}_r^2 + \sum_j |\bar{r}_j - \bar{r}|^{-1}\} | X_o \rangle . \tag{2.15}$$

ε_a is the valence-electron eigenvalue, and Z represents the nuclear charge.

The following model potential (V_m) was chosen for numerical calculations:

$$\begin{aligned} V_m(r) = {} & V_c(r) + (C_1 + C_2 r)\exp\{-r/r_o\} \\ & -(1/2)\alpha_d\, r^{-4}\{1-\exp[-(r/r_1)^6]\} \\ & -(1/2)C_3 r^{-6}\{1-\exp[-(r/r_1)^8]\}, \end{aligned} \tag{2.16}$$

where V_c represents the single particle central field potential and α_d is the static dipole polarizability of the core. The fourth term includes both the quadrupole interaction and the diabatic coupling between the valence electron and core. The parameters r_o and r_1 are chosen initially and the C_j's are chosen to reproduce the observed cesium term values. V_{so} represents the spin orbit potential and is given by

$$V_{so} = (1/2)\alpha^2(\bar{\ell} \cdot \bar{s})\xi r^{-3}, \qquad (2.17)$$

where α is the fine structure constant, $\bar{\ell}$ and $\bar{s}$ are the orbital and spin angular momentum of the valence electron, respectively, and ξ represents the effective nuclear charge. The valence electron orbitals can now be obtained from the numerical solutions of the following equation,

$$\left[-\frac{1}{2}\bar{\nabla}_r^2 + V_m(r) + V_{so}(r) - \varepsilon \right] \psi_a(\bar{r}) = 0. \qquad (2.18)$$

Adopting the notation that ψ_a represents the normalized, bound state wavefunctions with eigenvalues ε_a and ψ_ε represents the continuum wavefunction with eigenvalue $(\frac{1}{2})k^2$ for the usual energy delta function normalization, the photoionization cross section of the $Cs(6^2P_j)$ fine structure levels are now given by

$$\sigma_j(\ell'j') = 4\pi^2\alpha(\varepsilon-\varepsilon_j)|\bar{M}_{\ell',j',j}|^2[3(2j+1)]^{-1} \qquad (2.19)$$

where primes denote upper states. $\bar{M}$ is the dipole transition moment written as

$$\bar{M}_{ba} = \langle \Psi_b | \{ -\bar{r} - \sum_j \bar{r}_j \} | \Psi_a \rangle . \tag{2.20}$$

Substitution of Ψ_a and Ψ_b in this equation yields

$$\bar{M}_{ba} = \langle \Psi_b | \bar{Q}(\bar{r}) | \Psi_a \rangle , \tag{2.21}$$

where $\bar{Q}(\bar{r})$ is the effective dipole operator,

$$\bar{Q}(\bar{r}) = \langle X_o | \{ -\bar{r} - \sum_j \bar{r}_j \} | X_o \rangle = -\bar{r} - \langle X_o | \sum_j \bar{r}_j | X_o \rangle . \tag{2.22}$$

For large r,

$$\bar{Q}(\bar{r}) = -\bar{r}(1 - \alpha_d r^{-3}), \tag{2.23}$$

and for small r,

$$Q(r) = -r\{1 - \alpha_d r^{-3}[1 - e^{-(r/r_c)^3}]\}, \tag{2.24}$$

where r_c is the effective core radius. r_c was adjusted to predict the measured zero point of the Fano[19] polarization parameter for photoionization of ground state cesium atoms.

If R_j is chosen to represent the bound radial wave function and $R_{\ell',j'}$ the continuum radial wave function, then

$$|\bar{M}_{\ell',j',j}|^2=\max(1,\ell')(2j+1)(2j'+1)\begin{bmatrix} 1 & j & 1/2 \\ j' & \ell' & 1 \end{bmatrix}^2$$

$$x|<R_{\ell',j'},|\bar{Q}(\bar{r})|R_j>|^2. \qquad (2.25)$$

Using this in Eq. (2.19), the desired cross sections can now be determined.

Employing this method Weisheit[2] determined the photoionization cross section for the $6^2P_{3/2}$- and $6^2P_{1/2}$-states. The results are shown in Figs. 3a and 3b. For comparison the results of Norcross[17], who used a slightly different potential are included. Close agreement between the two theories is observed.

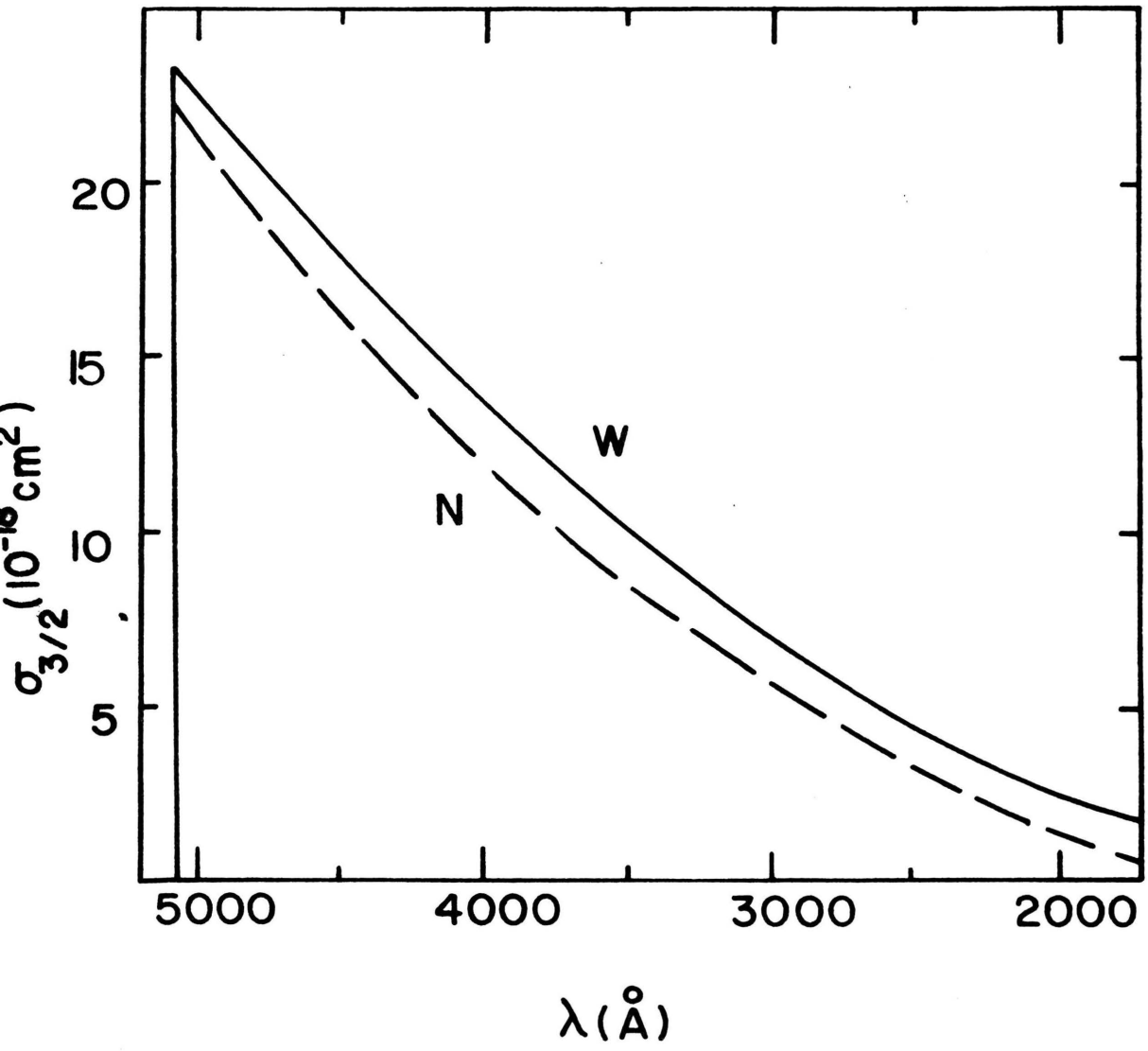

Fig. 3a. Theoretical photoionization cross sections of the $6^2P_{3/2}$-state of cesium. The curves result from Model potential calculations by Weisheit[2] (solid line) and Norcross[17] (dashed line).

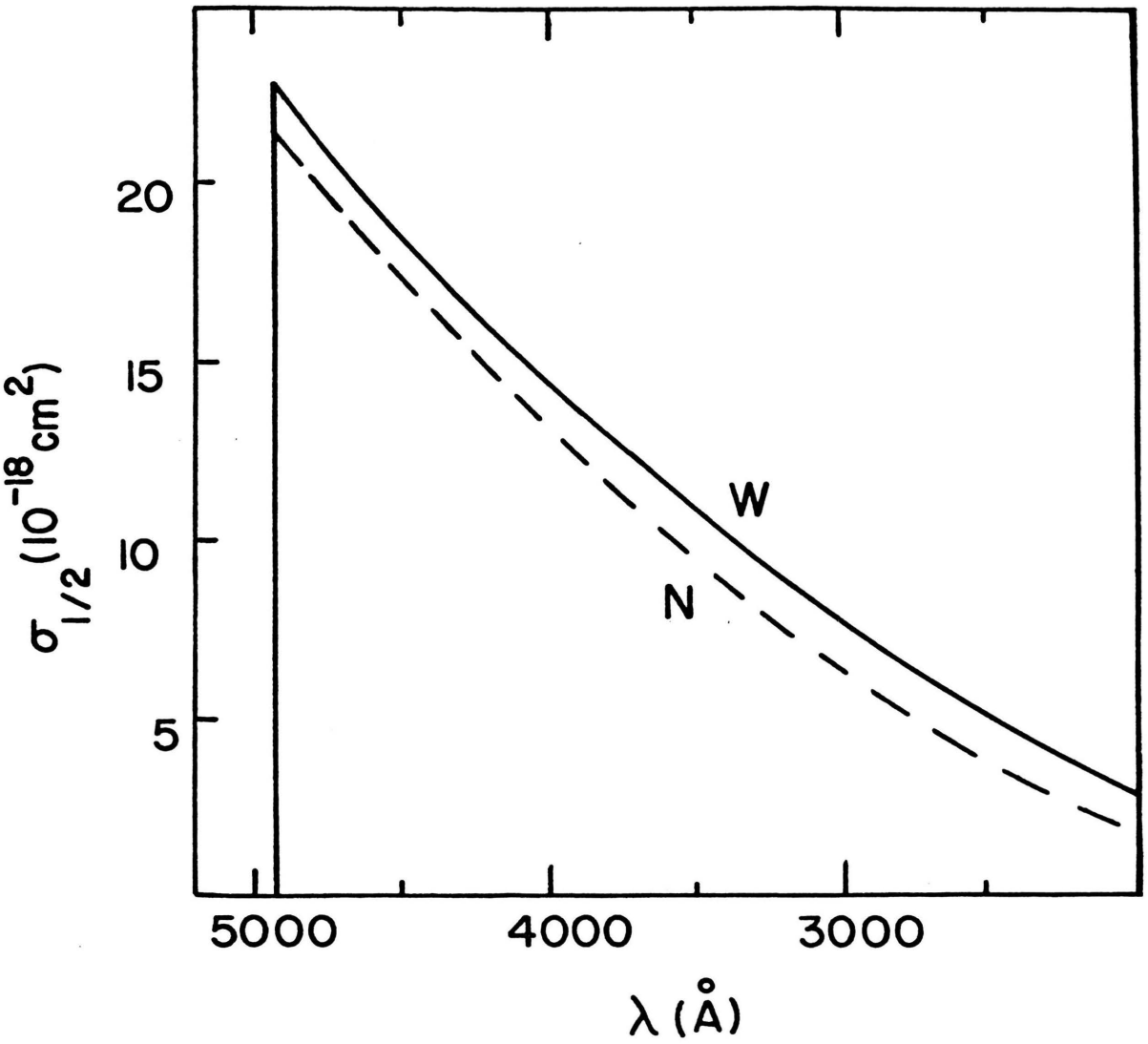

Fig. 3b. Theoretical photoionization cross sections of the $6^2P_{1/2}$- state of cesium. The curves result from Model potential calculations by Weisheit[2] (solid line) and Norcross[17] (dashed line).

III. EXPERIMENTAL ARRANGEMENT

A schematic diagram of the apparatus is shown in Fig. 4. The entire system is housed in an evacuated chamber of background pressure on the order of 10^{-9} torr. The cold surface is kept at liquid nitrogen temperature to minimize the coating of insulating surfaces with cesium. The atomic beam passes through the region labeled "interaction region" and is intersected by the two photon beams at this point. Also indicated in this diagram are the tungsten wire (filled circle) and the collector plate of the surface ionization detector (SID). In the following the major parts of the apparatus are described in more detail.

A. Atomic Beam

The atomic beam is produced in a two-stage oven. The first stage is a reservoir made of an oxygen-free, high-conductivity (OFHC) copper "pinch-off" tube. A commercially available glass ampule containing two grams of 99.9% pure cesium is inserted into the "pinch-off" tube prior to baking the whole system at 200^{o}C for 36 h. (We note that impurities are of no importance in this experiment since they are not excited by the cesium resonance radiation.) After vacuum is attained, the glass ampule is broken by squeezing the "pinch-off" tube. The number density of cesium atoms in the reservoir is controlled by external heating of the tube and varies with temperature as shown in Fig. 5. For

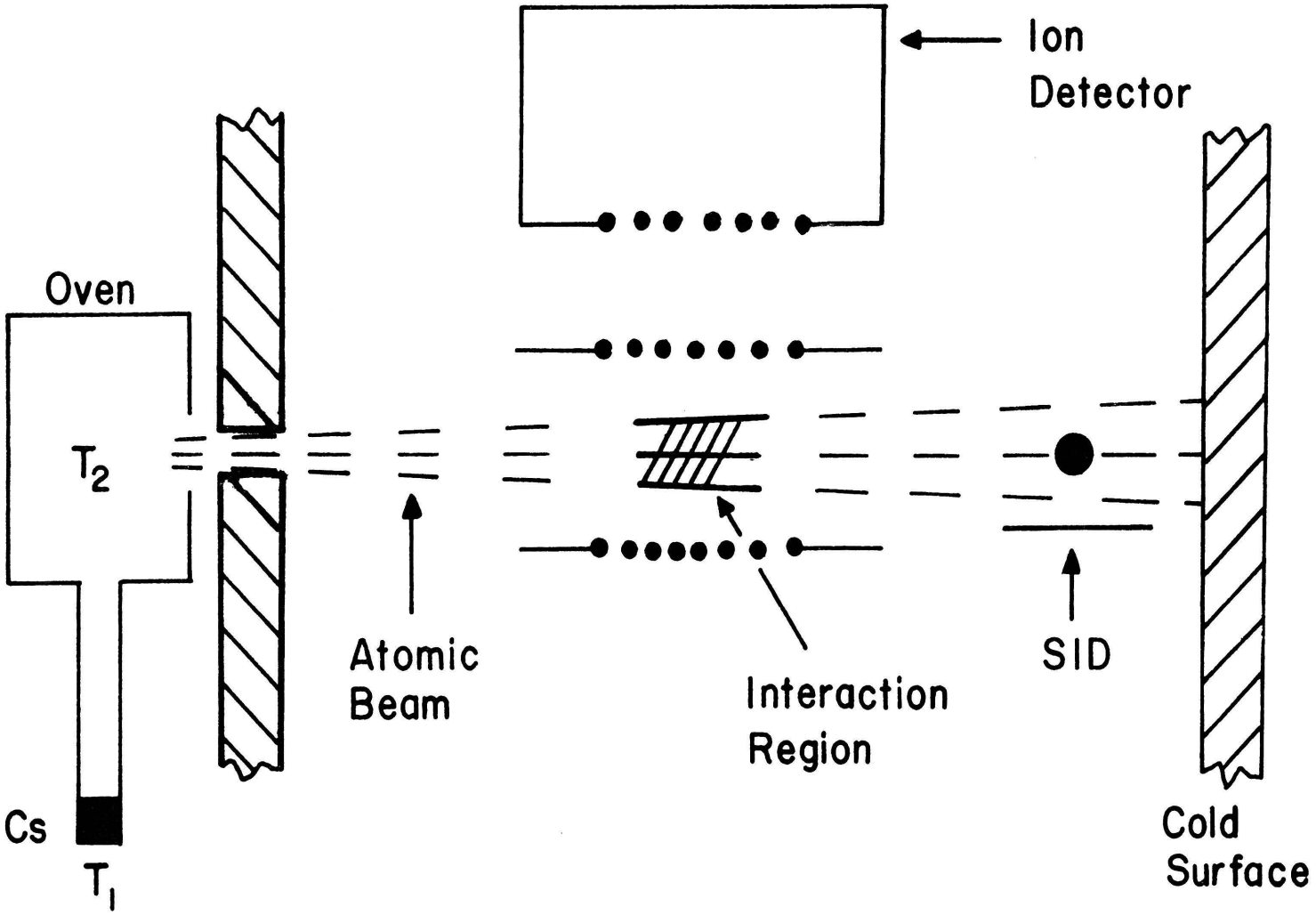

Fig. 4. Schematic diagram of the apparatus.

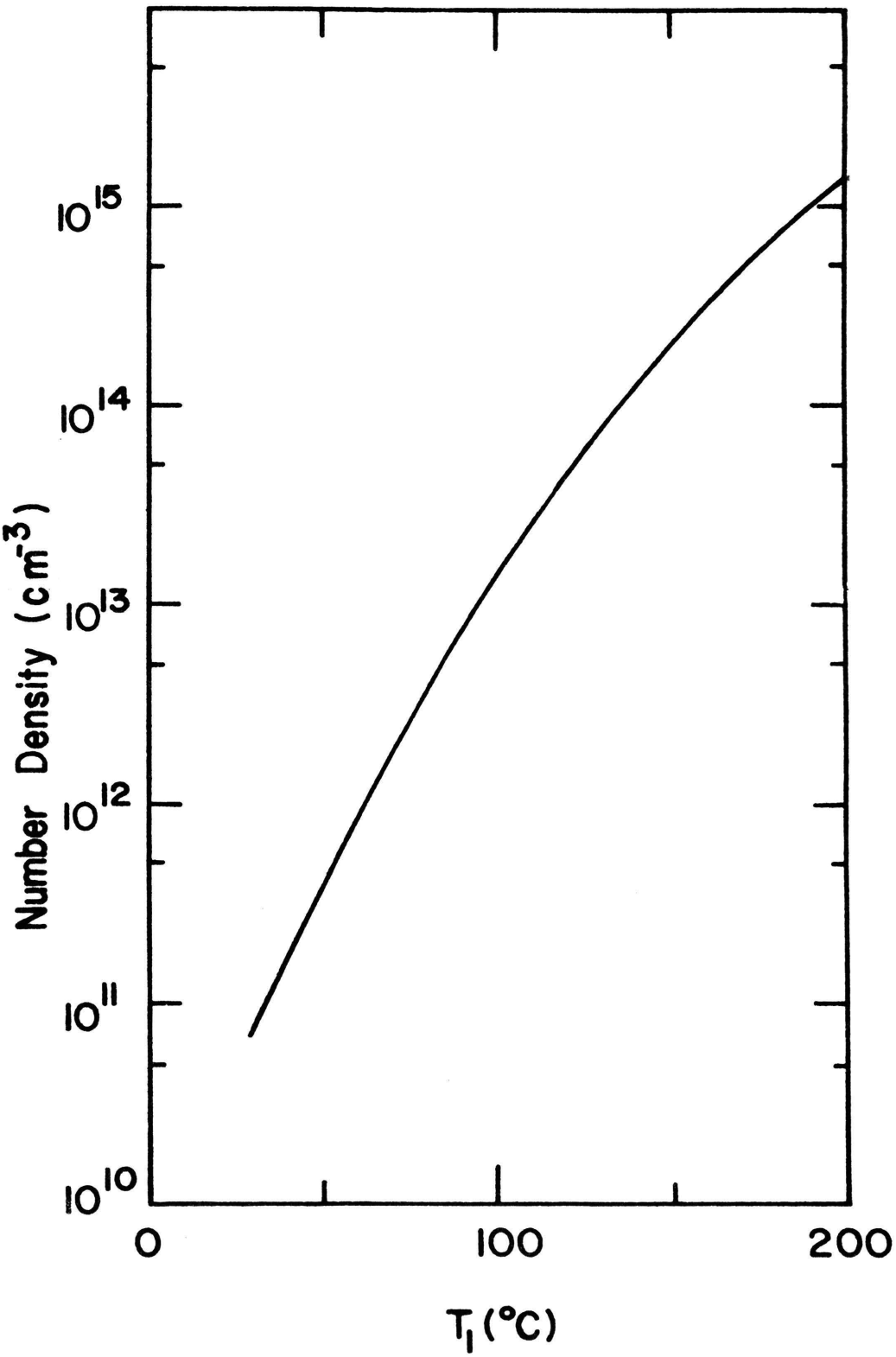

Fig. 5. Number density of cesium atoms in the oven reservoir as a function of temperature.

the purpose of the present work, T_1, the reservoir temperature was kept at a constant 125°C.

The second stage is the oven proper and consists of a thick-walled stainless steel tube covered at the end by a collimating hole structure (CHS)[20] of 1 in^2 surface area. This part of the oven is heated by a molybdenum wire filament and maintained at a temperature T_2 of 150°C. The resultant, directed, uniform density, atomic beam is further collimated by a 1 cm^2 aperture in the cold surface.

Although it is possible to calculate the number density of the atomic beam[21], it is more convenient to directly measure the beam density with a surface ionization detector (SID). The SID consists of a hot tungsten filament placed in the path of the atomic beam and a collector plate for the emitted cesium ions. Although the exact mechanism of this ionization process is not completely understood, it is generally assumed that ionization results from a tunneling of the outer shell electron of the atom to the surface[22]. This process is energetically favored if the work function of the metal is greater than the ionization potential of the atom, which is the case in the present work. A typical positive ion current, I^+(SID) as a function of filament temperature is shown in Fig. 6, where the temperature of the filament is determined from the tables of Jones and Langmuir[23]. The number density of neutral cesium atoms can

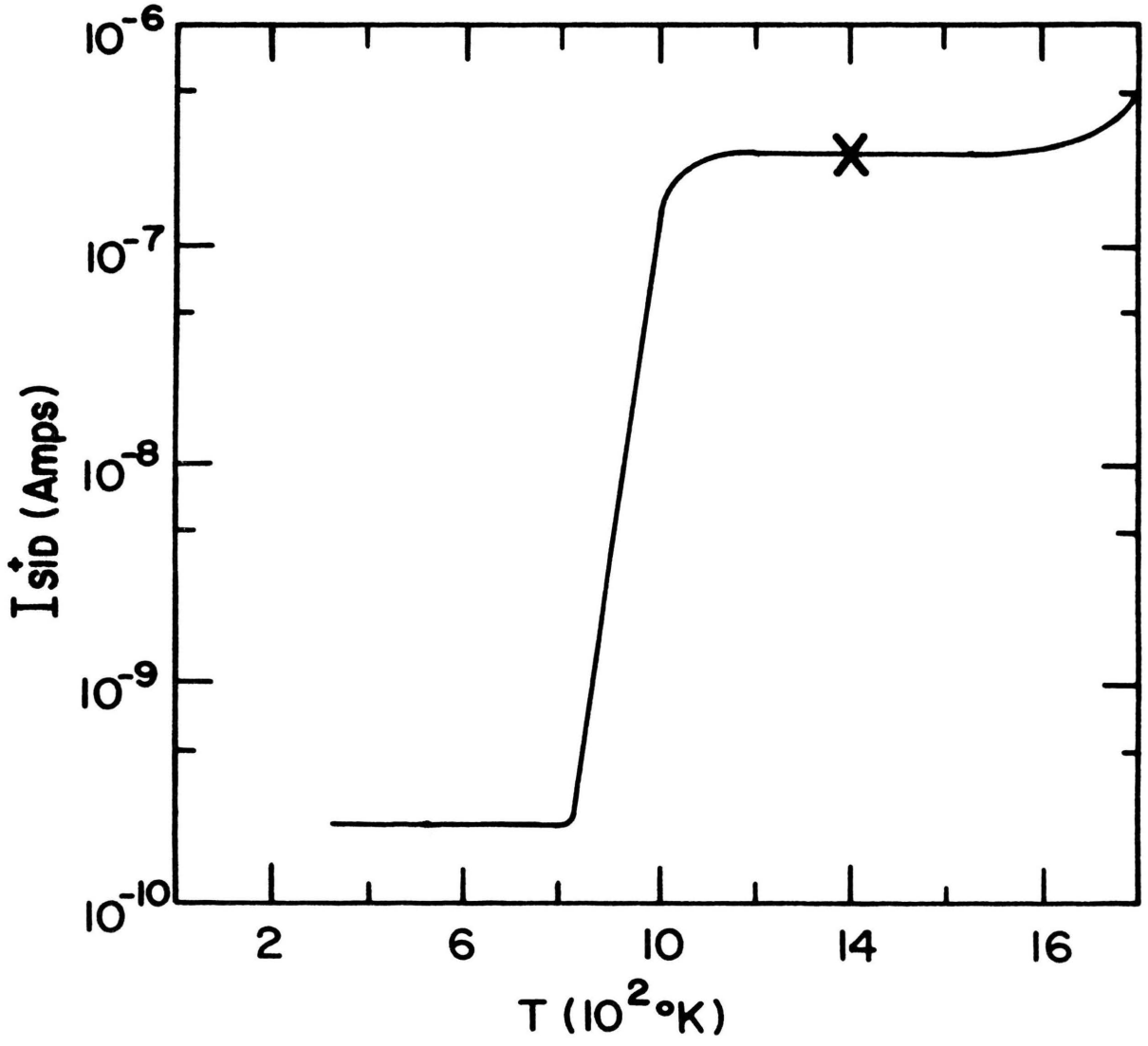

Fig. 6. Positive ion current of the SID as a function of the filament temperature. The current plateau shown corresponds to an atomic beam density of 3×10^{10} cm^{-3}. The operating point is indicated by an X.

then be calculated from the relationship,

$$I^{+}(SID) = \phi\ n_o \langle v \rangle d\ell e\ , \qquad (3.1)$$

where ϕ is the ion production efficiency, (equals one for cesium[24]), n_o is the number density of ground state cesium atoms, $\langle v \rangle$ is the average velocity of the atomic cesium, ℓ and d are the length and diameter of the wire respectively and e is the charge of the ion. A typical number density measured for the present experiment is 3×10^{10} cm^{-3}.

An independent check on the proper operation of the SID is to measure the electron emission current from the hot filament in the presence of the atomic beam as a function of the inverse filament temperature. The results of this measurement is the characteristic Langmuir S-curve[25] shown in Fig. 7.

B. Light Sources

It can be seen by solving Eq. (1.4) for $N^{+}(\lambda)$ that the number of photoionization events in the apparatus is directly proportional to the photon fluxes $j_1(\lambda_o)$ and $j_2(\lambda)$ of the excitation and ionization light source, respectively. Therefore some care must be taken to find light sources of reasonable stability and intensity as discussed below.

Light sources for the excitation radiation should provide the two resonance wavelengths, 8521 and 8944 $\mathring{A}$ for the photoexcitation to the fine structure levels. A pulsed GaAs

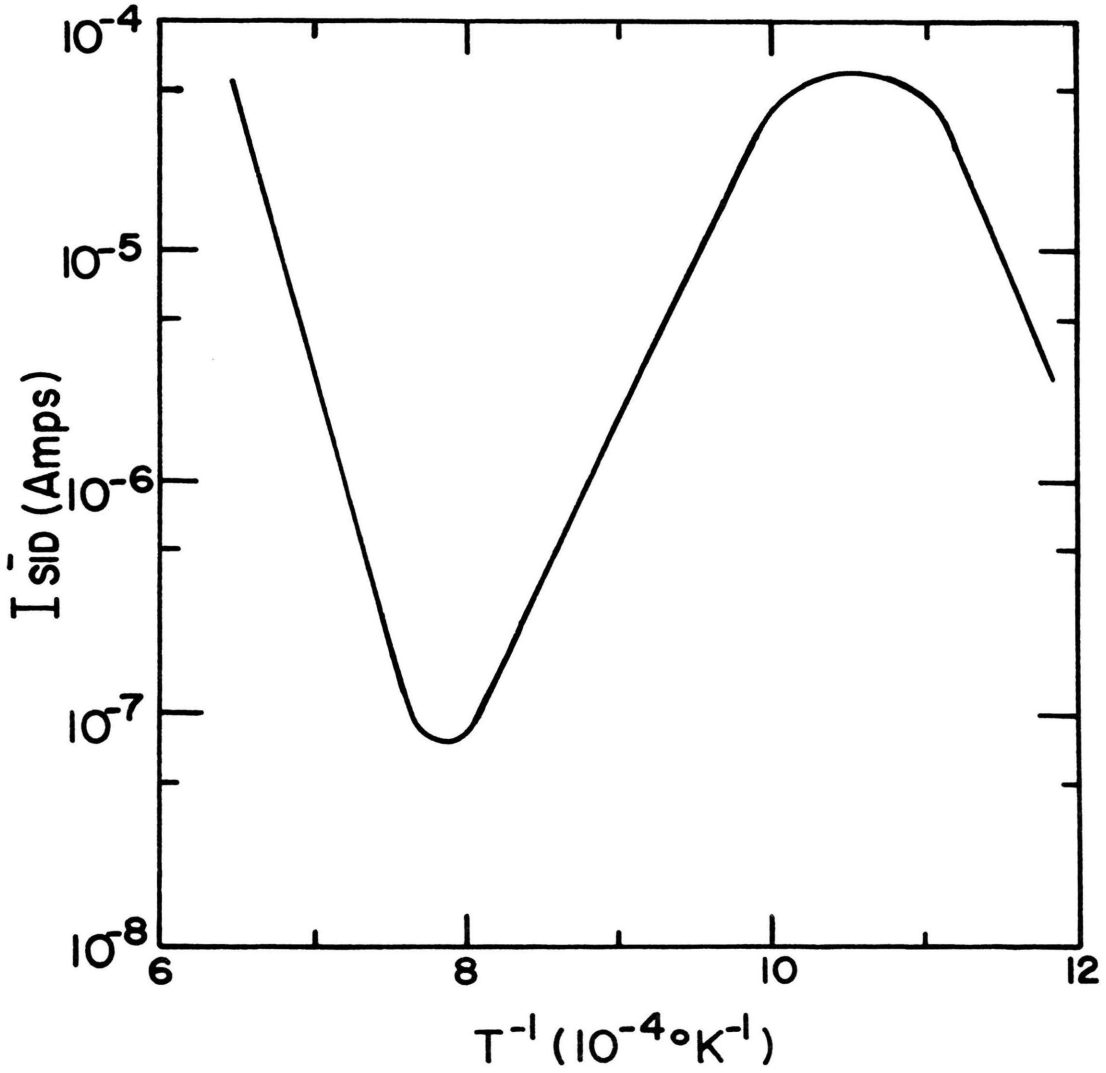

Fig. 7. Electron emission current from the SID filament as a function of the inverse temperature of the filament. It shows the characteristic Langmuir S-curve. During this measurement the filament was exposed to a beam of cesium atoms of density 3×10^{10} cm^{-3}.

laser[26,27] was initially considered for this source, and even though the photon flux per pulse was adequate, it was deemed unsatisfactory due to problems encountered with stability and frequency tuning.

The light source finally chosen was a commercial dc cesium discharge lamp[28], which produced sufficient photon flux in the two resonance lines. The desired line was selected with the aid of an interference filter.

A high pressure mercury-xenon (Hg-Xe) lamp[29] was chosen for the ionization light source. It contains several intense spectral lines between 5500 and 2500 Å, superimposed on a strong continuum. The main disadvantage of this lamp was the absence of sharp lines near threshold, around 5000 Å.

A quarter meter, high intensity monochromator was used to isolate the strong lines of the Hg-Xe lamp. A compromise between resolution and high photon flux resulted in a full-width half-maximum line profile of 150 Å. Calibrated photodiodes[30] were used to determine the relative intensities of the spectral lines. From these intensities the photon flux $j_2(\lambda)$ can be calculated.

C. Ion Extraction and Detection

The interaction region where the three beams overlap has a volume of approximately 0.1 cm^3. The series of parallel wire mesh grids (see Fig. 4) are biased to attract ions to the entrance grid of the particle detector. The

wire mesh is approximately 80% transmitting and has an area much larger than the interaction region, thereby assuring a high collection efficiency for ions.

Ions passing the entrance grid to the ion detection region are accelerated towards a twenty stage focused-mesh, Cu-Be electron multiplier with a 1 in^2 active counting area[31]. Pulses from the multiplier are counted as described below.

D. Counting System

A block diagram of the pulse-shaping and counting network is shown in Fig. 8. After processing, the pulses are fed into a Digital Synchronous Computer (DSC). The DSC[32] is a two-scaler counter with the feature that each channel may be independently gated "open" to accept pulses for a pre-set, non-overlapping time interval. The reference signal used to gate the DSC is derived from a photodiode modulated by the excitation radiation mechanical chopper. During the "on" portion of the chopper cycle the excitation radiation passes through the interaction region and both background and signal events are recorded. The excitation source is blocked during the "off" portion of the cycle so only background events are recorded. The pre-set counting time for each channel was 45 msec and the modulation frequency was 10 Hz. Under proper operating conditions the difference of the counts stored in the two channels is interpreted as the number of two-step

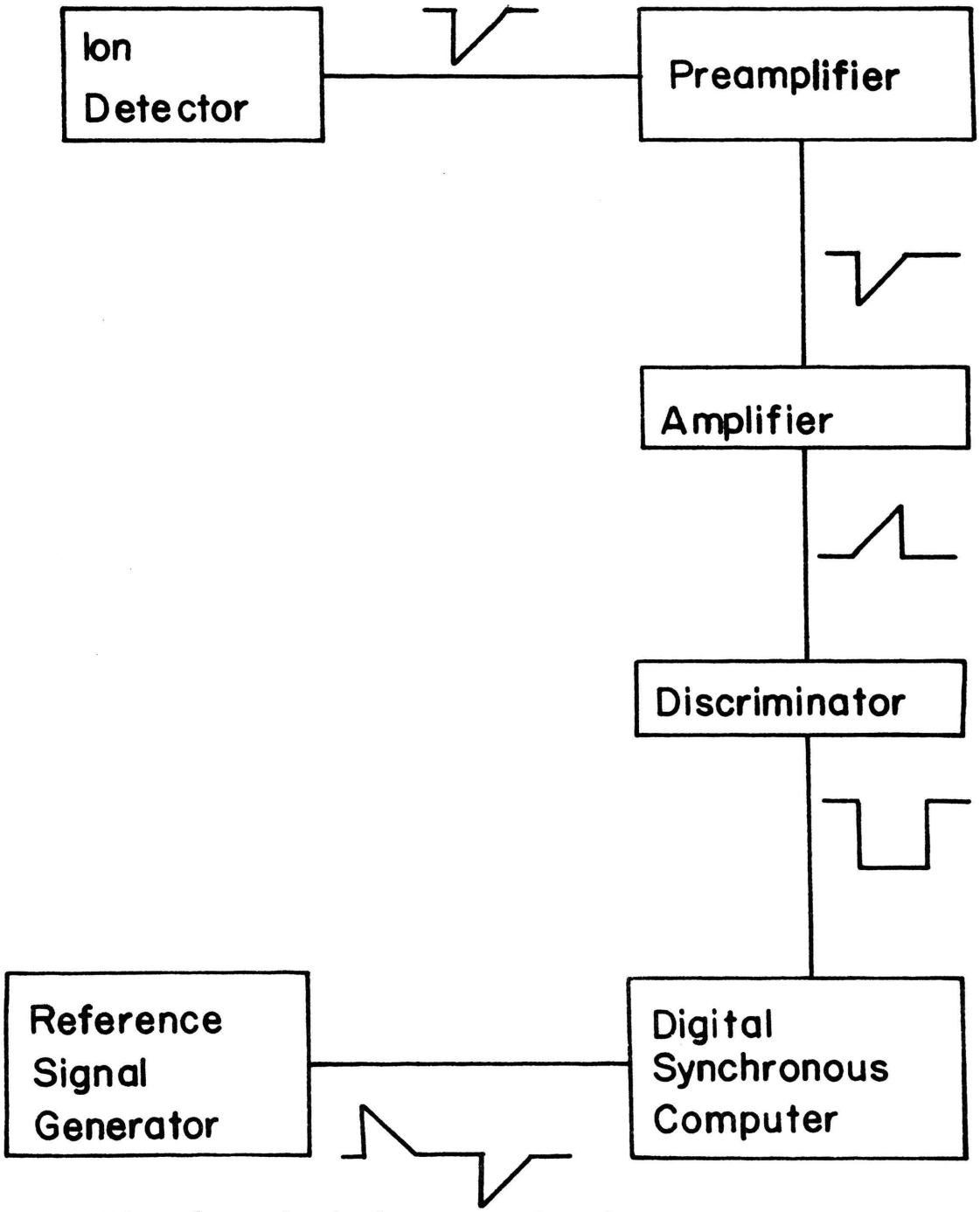

Fig. 8. Block diagram of pulse counting network. All pulses are drawn with positive potential upward.

photoionization events that occurred during the counting time. Thus the effects of slow drifts in background counts are minimized and long data acquisition times are possible. These techniques have allowed reliable signal detection for signal-to-noise ratios as small as $1:10^3$.

IV. EXCITATION AND IONIZATION PROCESSES

A. Production of Excited Atoms

As can be seen from Eq. (1.4) the cross section is directly proportional to the number of ions produced in the two-step photoionization process. The number of ions produced will in turn be directly proportional to the number of atoms in the excited state. It is, therefore, relevant to consider this excitation process in detail and estimate the number of excited atoms present in this experiment.

The excitation radiation is attenuated as it passes through the atomic beam according to

$$j_\nu(\ell) = j_\nu(0)e^{-k'_\nu \ell}, \tag{4.1}$$

where $j_\nu(0)$ and $j_\nu(\ell)$ represent the incident and transmitted photon flux per frequency interval, ℓ is the distance traveled through the atomic beam, and k'_ν is the absorption coefficient. The number of photons absorbed per cm^3 per sec is

$$\frac{dn_p}{dt} = \frac{j_\nu(0)}{\ell}\left[1-e^{-k'_\nu \ell}\right]. \tag{4.2}$$

Thus the rate equation for the production of excited atoms can be written as

$$\frac{dn^*_\nu}{dt} = -\frac{n^*_\nu}{\tau} + \frac{j_\nu(0)}{\ell}\left[1-e^{-k'_\nu \ell}\right]. \tag{4.3}$$

The steady state solution is

$$n_\nu^* = \frac{\tau j_\nu(0)}{\ell} [1-e^{-k'_\nu \ell}]. \tag{4.4}$$

The total number of atoms in the excited state can be found by integrating over all frequencies. Since k'_ν will be small in the present study, the exponential may be approximated by a Taylor's series. Keeping only the first two terms of the expansion and integrating, Eq. (4.4) yields

$$n_\nu^* = \tau \int_o^\infty j_\nu(0) k'_\nu \, d\nu \tag{4.5}$$

The spectral distribution of the incident photon flux is the same as the emission profile of the excitation lamp. Since the excitation lamp used in this study was a low-pressure cesium dc discharge without any buffer gas, line broadening of the emitted spectral lines was due primarily to Doppler broadening, and can be written[33]

$$j_\nu(0) = C_o \, e^{-\omega^2} \tag{4.6}$$

where C_o is a constant which is found by normalizing the total photon flux to the observed photon flux, $j_1(\lambda_o)$ of the resonance line λ_o, viz.,

$$\int_o^\infty j_\nu(0) d\nu = j_1(\lambda_o). \tag{4.7}$$

The quantity ω is given by

$$\omega = \frac{2(\nu-\nu_o)}{\Delta\nu_{D\ell}} \sqrt{\ell n 2} \ , \tag{4.8}$$

where ν_o is the resonance frequency and $\Delta\nu_{D\ell}$ is the Doppler line width. It is possible to calculate $\Delta\nu_{D\ell}$ from

$$\Delta\nu_{D\ell} = 2\left[\frac{2kT}{m} \ \ell n 2\right]^{1/2} \frac{\nu_o}{c} \ , \tag{4.9}$$

where k is Boltzmann's constant, T is the absolute temperature, m is the molecular weight, and c represents the speed of light.

In the atomic beam, broadening of the absorption line will again be entirely due to Doppler broadening. It should be pointed out that not only is the line broadened but it is also shifted due to the Doppler effect since the two beams cross at an angle of 60^o with respect to each other. The quantity k'_ν can be expressed as

$$k'_\nu = k_o e^{-\omega'^2} \tag{4.10}$$

where ω' is given by

$$\omega' = \frac{2(\nu-\nu_o)}{\Delta\nu'_{Da}} \sqrt{\ell n 2} \tag{4.11}$$

$\Delta\nu'_{Da}$ represents the apparent Doppler width of the absorption line. The maximum value of the absorption

coefficient, k_o, can be calculated from

$$k_o = \frac{2}{\Delta\nu'_{Da}} \left(\frac{\ell n 2}{\pi}\right)^{\frac{1}{2}} \frac{\lambda_o^2}{8\pi} \frac{g_2}{g_1} \frac{n_o}{\tau} , \tag{4.12}$$

where n_o is the number density of ground state atoms in the atomic beam and g_1 and g_2 represent the statistical weights of the ground and excited states, respectively. The ratio g_2/g_1 for cesium ($6^2P_{3/2}$) is 2.

In Eq. (4.11) and (4.12) the apparent Doppler width (the Doppler width seen by the excitation radiation) is related to the actual Doppler width, $\Delta\nu_{Da}$, by

$$\Delta\nu_{Da}' = \Delta\nu_{Da}\left[1 - \frac{\langle v \rangle}{c} \cos \zeta\right], \tag{4.13}$$

where $\langle v \rangle$ is the velocity of the atomic beam, and ζ represents the angle between the atomic beam and the excitation radiation. The actual Doppler width can be calculated from

$$\Delta\nu_{Da} = 2\left[\frac{2kT_2}{m} \ell n 2\right]^{\frac{1}{2}} \frac{\nu_o}{c} , \tag{4.14}$$

where T_2 represents the temperature of the atomic beam.

In the present experiment the following approximate numbers prevail:

$$\zeta = 60^{o}$$

$$\ell = 1 \text{ cm}$$

$$T_1 = 375^{o}K$$

$$T_2 = 425^{o}K$$

$$\langle v \rangle = 3.19 \times 10^{4} \text{cm sec}^{-1}$$

$$\nu_o = 3.5 \times 10^{14} \text{ sec}^{-1}$$

$$\Delta\nu_{D\ell} = 4.2 \times 10^{8} \text{ sec}^{-1}$$

$$\Delta\nu_{Da} = 4.5 \times 10^{8} \text{ sec}^{-1}$$

$$k_o = 0.4 \text{ cm}^{-1}$$

$$\tau = 3 \times 10^{-8} \text{ sec}$$

$$n_o \approx 10^{10} \text{ cm}^{-3}$$

$$j_1 \approx 10^{15} \text{ cm}^{-2} \text{ sec}^{-1}$$

Substitution of the above numbers in Eq. (4.5) yields an excited state number density of $\approx 10^{5}$ cm^{-3}. Even with this low density of excited atoms the cross section can be measured as discussed in the following paragraph.

B. Production of Ions

The rate at which ions are produced at a wavelength λ per wavelength interval from the excited state can be written

$$\frac{dn^{+}_{\lambda}}{dt} = n^{*}\sigma(\lambda)j_2'(\lambda), \tag{4.14}$$

where $\sigma(\lambda)$ is the photoionization cross section from the excited state and $j_2'(\lambda)$ represents the photon flux per wavelength interval from the ionization light source. The

number of ions produced per second per wavelength interval, $N^+(\lambda)$, in an interaction volume V is

$$N^+(\lambda) = \frac{dn^+(\lambda)V}{dt} = n^*\sigma(\lambda)j_2'(\lambda)V. \qquad (4.15)$$

The total number of ions produced can be found by integrating the above equation over the full bandwidth of the ionization light source, $2\Delta\lambda$.

$$\int_{\lambda_2-\Delta\lambda}^{\lambda_2+\Delta\lambda} N^+(\lambda)d\lambda = n^*V \int_{\lambda_2-\Delta\lambda}^{\lambda_2+\Delta\lambda} \sigma(\lambda)j_2'(\lambda)d\lambda, \qquad (4.16)$$

where λ_2 represents the center wavelength and $\Delta\lambda$ is the half width. The left side of this equation will be just the total number of ions produced, $N^+(\lambda_2)$, over the bandwidth $2\Delta\lambda$ centered about λ_2. If it is assumed that $\sigma(\lambda)$ is a constant over the bandwidth and has the value $\sigma(\lambda_2)$, which is a good approximation since $\sigma(\lambda)$ is slowly varying[1-4] and only a relatively small wavelength interval is being considered, then Eq. (4.16) becomes

$$N^+(\lambda_2) = n^*V\sigma(\lambda_2) \int_{\lambda_2-\Delta\lambda}^{\lambda_2+\Delta\lambda} j_2'(\lambda)d\lambda. \qquad (4.17)$$

The integral in Eq. (4.17) represents the total photon flux observed over the wavelength interval. Then the total

number of ions produced is

$$N^+(\lambda_2) = n^*V\sigma(\lambda_2)j_2(\lambda_2). \qquad (4.18)$$

An order of magnitude estimate for $N^+(\lambda_2)$ can now be made. Assume an interaction volume of 0.1 cm^3, a cross section of 6×10^{-18} cm^2, and a photon flux of 5×10^{14} $cm^{-2}sec^{-1}$, which are approximate values at $\lambda = 4360$ Å. The estimated value of $N^+(\lambda_2)$ is 50 ions per sec., and the observed count rate is 5 per sec. This indicates an ion counting efficiency of approximately 10%. However, it must be remembered that the above is an estimate of $N^+(\lambda_2)$ only.

C. Competing Processes

Along with the two-step ionization process there are additional processes which can produce ions in the apparatus. The following is an enumeration of these processes and an attempt to estimate their contribution to the observed count rate. It should be emphasized that modulation of the excitation radiation results in cancellation of the effects of most spurious ions. The primary competing processes are discussed below:

1. $Cs^* + Cs \rightarrow Cs_2^+ + e^-$

This effect can readily be discounted because the collision frequency in an atomic beam is extremely small. Also the lifetime of the excited state is only about 30 nsec.

2. $Cs_2 + h\nu \rightarrow Cs_2^+ + e^-$

The cross section for photoionization of the cesium dimer has been studied and found to be of the same order of magnitude as the cross section for Cs^{*}[34]. The contribution due to this process is eliminated in the present apparatus because it would be an effect associated with the ionization radiation only.

3. $Cs + e^- \rightarrow Cs^+ + 2e^-$

The cross section for this reaction has been studied[35-38] and is significant. In the present apparatus large numbers of secondary electrons are liberated from cesiated surfaces by the incident radiation. These electrons can be accelerated through the interaction region giving rise to electron impact ionization. Ideally, the cross section for electron impaction ionization of ground state cesium atoms is zero if the energy of the electrons can be kept below the ionization threshold of 3.89 eV. In practice, however, greater ion collection efficiencies are attained for extraction fields of about 20 volts/cm in the interaction region. Although ions are produced from this process, the only noticeable effect is an increase in the background count rate, since it has been observed that no photoelectrons are liberated by the excitation light at wavelengths of 8944 and 8521 Å. Also, electron impact ionization of excited atoms can be ignored because of the low values of the photoelectron current and excited atom density.

4. $Cs + h\nu \rightarrow Cs^+ + e$

Photoionization of ground state atoms has been studied both experimentally and theoretically[9,14,39-42]. Although there is disagreement as to the value of the cross section for this effect, it is about two orders of magnitude lower than for Cs^*. However, the number density of ground state atoms is 10^5 times that of the excited state. This process adds considerably to the total count rate below 3189 Å, the ground state photoionization threshold, but is effectively discriminated against by the modulation scheme employed in the experiment.

5. $Cs^*(6P) + Cs^*(6P) \rightarrow Cs_2^+ + e$

The cross section for associative ionization has been studied[43-45] and found to be of the order of 10^{-18} cm^2. However, the collision frequency in an atomic beam is extremely small and this effect has not been observed in the present experiment.

6. (Cesiated Surface) $+ h\nu \rightarrow Cs^+ + e^-$

The photo-ionic effect from cesiated surfaces at room temperature is a controversial issue. Medicus and Breaux[46] have presented evidence in support of this process, but their analysis has been criticized by Shaw and Stickney[47]. In the present apparatus, the ionization light is collimated as much as practical, however, a portion of the

beam still strikes the ion extraction grids. It has been observed that before the cesium ampule is broken there is less than one background count per second with the light sources in place. After the ampule is broken and cesium is allowed to deposit on the electrodes, but without an atomic beam, there is an observed background count rate of approximately 500 per second. Although this experiment is not designed to study the photo-ionic effect, it is believed that the observed background count rate is due in part to this process. The net effect of this process is also eliminated since it is due entirely to the ionization radiation. More conventional surface effects like thermionic and photoelectric emission are also eliminated with our digital synchronous technique.

V. RESULTS AND DISCUSSION

A. Statistical Considerations

Due to the large total count rate, typically of the order of 500 per sec, and small net count rate, typically from 0.1 to 5 per sec, it is necessary to consider the statistical variations involved in acquiring data. The two step photoionization process as well as the various noise processes occurring in this experiment meet the following Poisson statistics criteria:

1. The chance of one atom undergoing an ion-producing interaction is the same for all atoms in the same group.
2. An interaction by one atom does not affect the chance that other atoms can have an interaction.
3. The chance of an interaction in a given time interval is equal for all time intervals.
4. The total number of atoms and the total number of equal time intervals are large.

The statistical error associated with counting events in general may be applied to the errors in each channel of the counter. According to Poisson statistics[48], the variance δ^2 may be written

$$\delta^2 = \sum_{x=0}^{\infty} \frac{(x-m)^2 m^x e^{-m}}{x!} = m \qquad (5.1)$$

where x is the observed counts within a certain time interval, and m is the true mean value of the counts. The standard error, or standard deviation from the mean, is the square root of the variance,

$$\delta = \sqrt{m} \ . \tag{5.2}$$

In practice, however, the true value is not known but can be approximated by the observed mean value <x>. If a large number of observations are taken,

$$\delta = \left(\frac{<x>}{n} \right)^{\frac{1}{2}} , \tag{5.3}$$

where n represents the total number of counting intervals.

In the present study n is large and may be directly related to time. Since it is necessary to make an observation for each channel before another observation of the first channel can be made, the total time required to make one observation is 0.1 sec, although the observation time is only 45 msec. Fig. 9 indicates the number of observations and the time required for these observations to obtain a given per cent error, for one channel, at various count rates. As indicated by Eq. (5.3) and Fig. 9, the per cent error decreases as the reciprocal of the square root of the counting time, i.e., in order to cut the statistical error by a factor of 2 it is necessary to count a factor of 4 times longer.

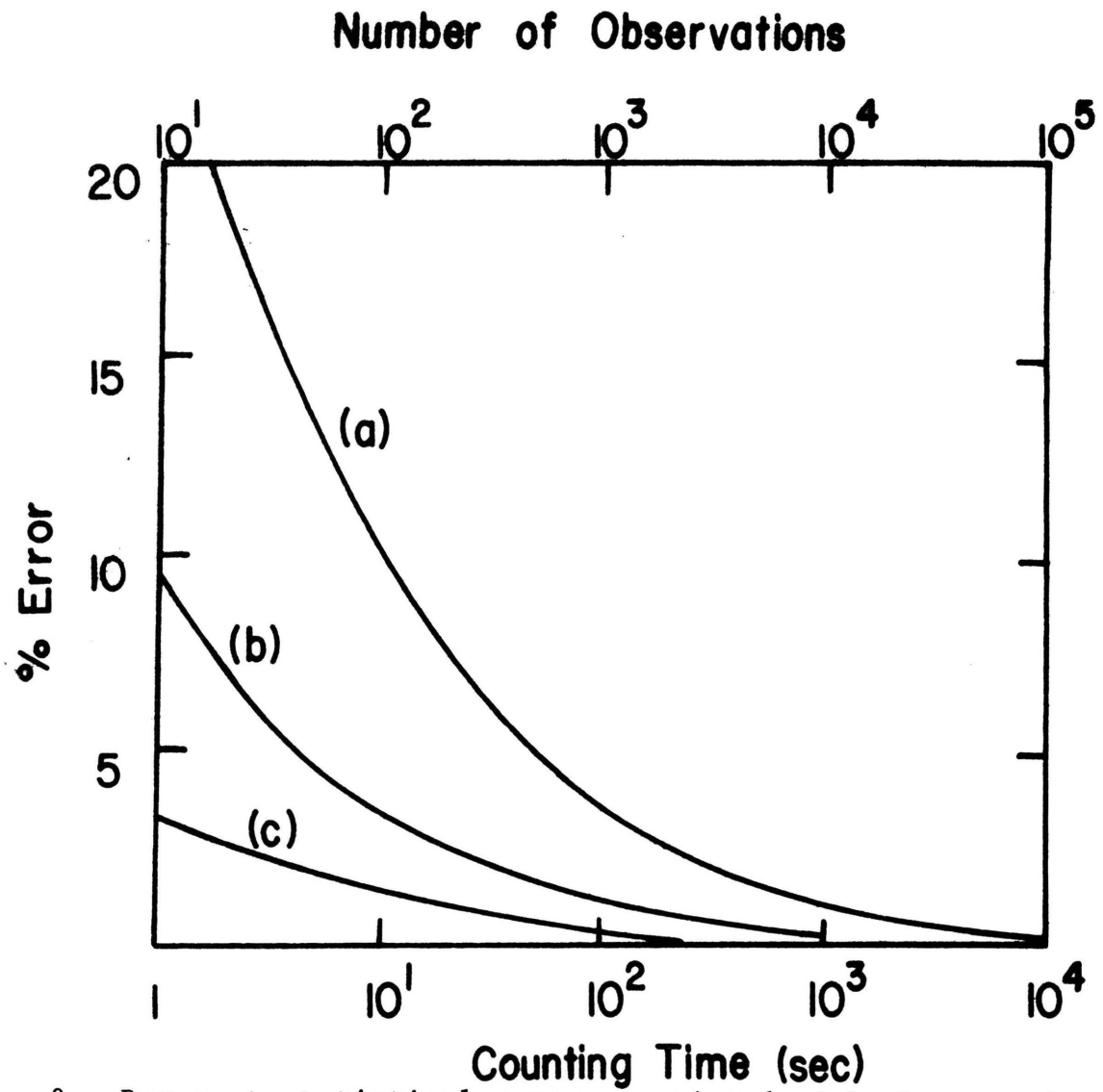

Fig. 9. Per cent statistical error associated with the counting of events as a function of the number of observations. This corresponds to the error associated with each channel of the Digital Synchronous Computer (DSC). The three curves are for count rates of (a) 10 (b) 100 and (c) 1000 counts/sec.

Now consider the statistical error associated with the subtraction of two large numbers which will correspond to the error associated with the net count rate. Denote the number of counts stored in the signal-plus-background and background-only channels by x and y with mean values of $\langle x \rangle$ and $\langle y \rangle$, respectively. Denote the difference of the two channels by z with average $\langle z \rangle$ and the observed net counts by N^+. Then

$$N^+ = \langle z \rangle \pm \delta_z,$$

where

$$\delta_z = (\delta^2_x + \delta^2_y)^{\frac{1}{2}} = \left(\frac{\langle x \rangle + \langle y \rangle}{n} \right)^{\frac{1}{2}} \qquad (5.4)$$

Fig. 10 indicates the number of observations and the time required for these observations to be within a given per cent error for the difference of the two channels at various signal-to-noise ratios. As before, from Eq. (5.4) and Fig. 10, it can be seen that the per cent error decreases as the reciprocal of the square root of the counting time.

In the remainder of this paper, we shall use the most probable error, β, defined as

$$\beta \equiv 0.6745\delta. \qquad (5.5)$$

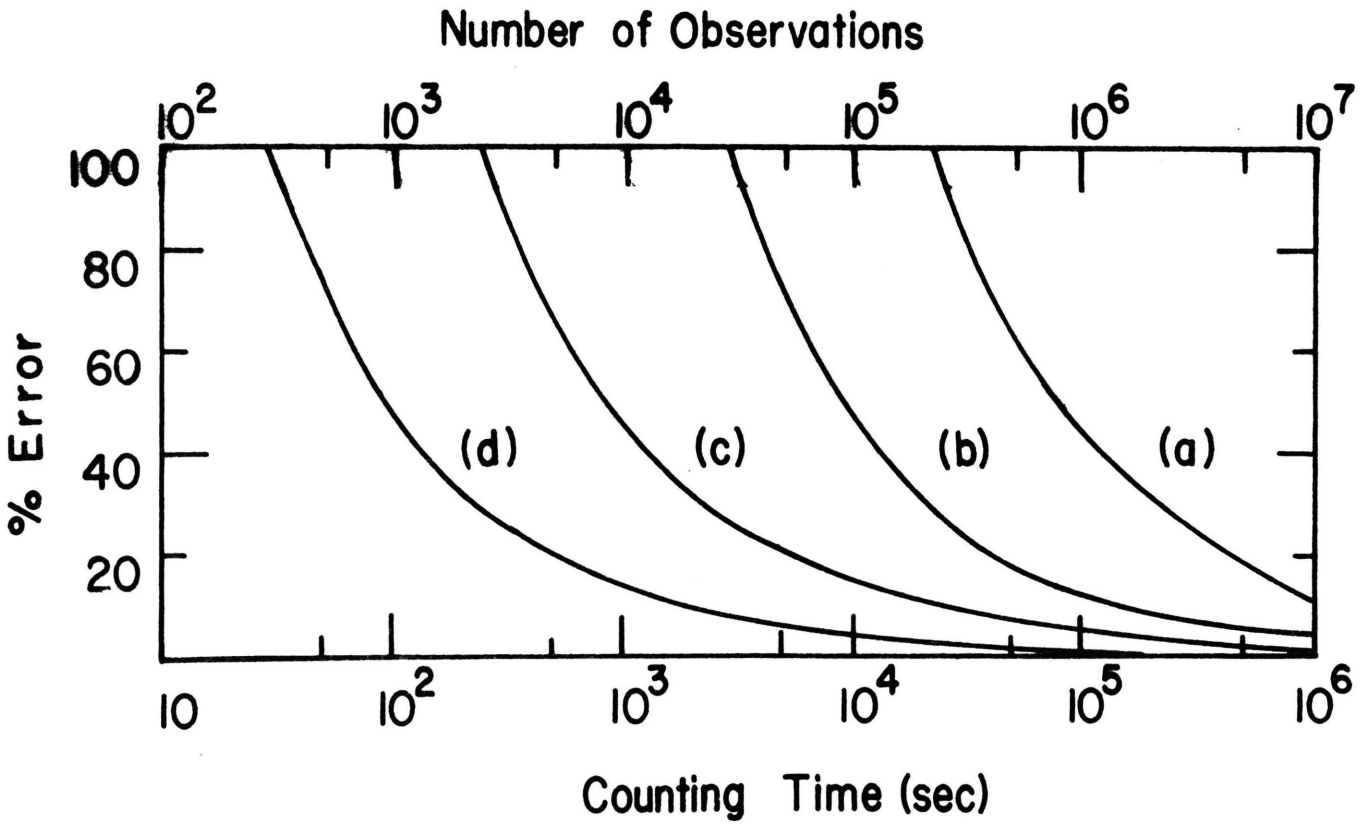

Fig. 10. Per cent statistical error associated with the subtraction of two statistical numbers as a function of the counting time or the number of observations. This corresponds to the error associated with the net count rate. Count rate from (a) to (d): 10^4, 10^3, 10^2, and 10 per sec. Signal-to-noise ratio from (a) to (d): 10^{-4}, 10^{-3}, 10^{-2}, 10^{-1}.

The meaning of the most probable error is that there is a 50% probability that the results of an identical measurement will lie within one standard deviation of the previous measurement.

B. Consistency Checks and Stability

According to Eq. (1.4), the number of ions produced is directly proportional to n_o, $j_1(\lambda_o)$, and $j_2(\lambda_2)$. Because of this relationship, the proper operation of the apparatus can be insured by reducing one of these quantities by a known percentage to determine if the net count rate is reduced by the same percentage. At various wavelength settings of the ionization light, neutral density filters were used to reduce $j_1(\lambda_o)$ or $j_2(\lambda_2)$. Typical results of these measurements are shown in Figs. 11 and 12. The observed values from these measurements are within statistical variation of the expected values for each case.

Formal consistency checks were not taken by varying n_o because of the time necessary for thermal stabilization of the oven and reservoir. Also, to measure n_o with the SID, it is necessary to turn off the ion extraction and counting system, which is undesirable during a series of data accumulation times. However, at various times the oven and reservoir temperatures were reduced and allowed to stabilize for a period of 10 hours and an appreciable decrease in the net count rate was observed.

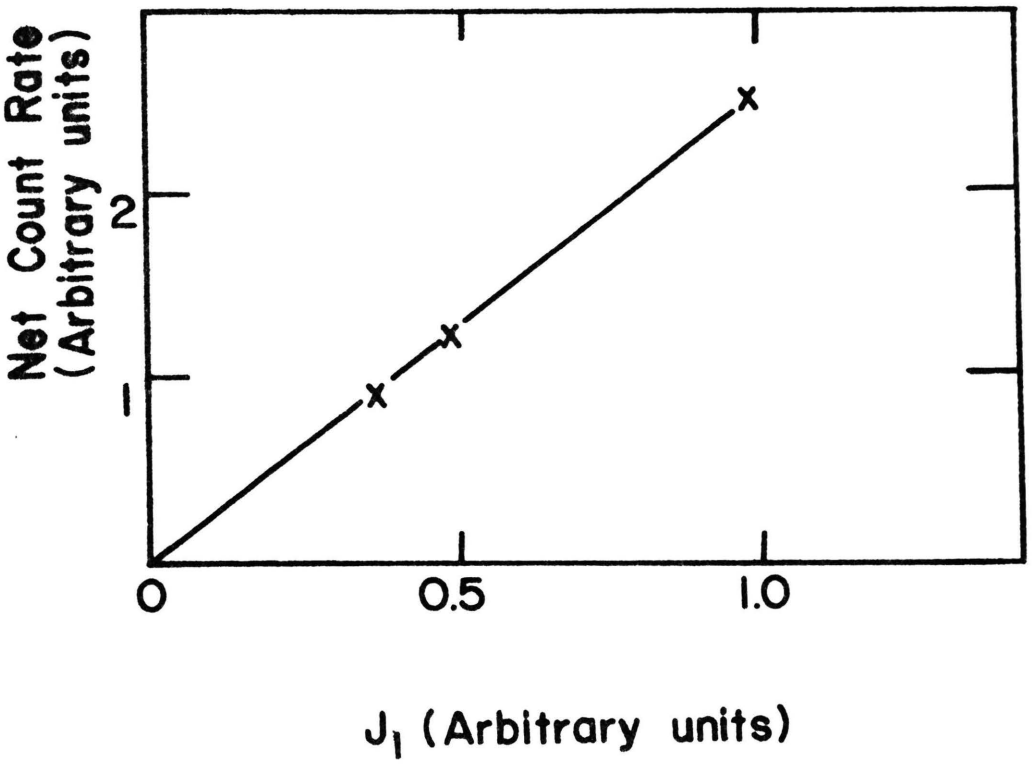

Fig. 11. Consistency check for the excitation radiation $j_1(\lambda_o)$. The dependence of the net count rate on the photon flux from the excitation radiation is shown. These measurements were taken at constant atomic beam density and constant photon flux from the ionization radiation.

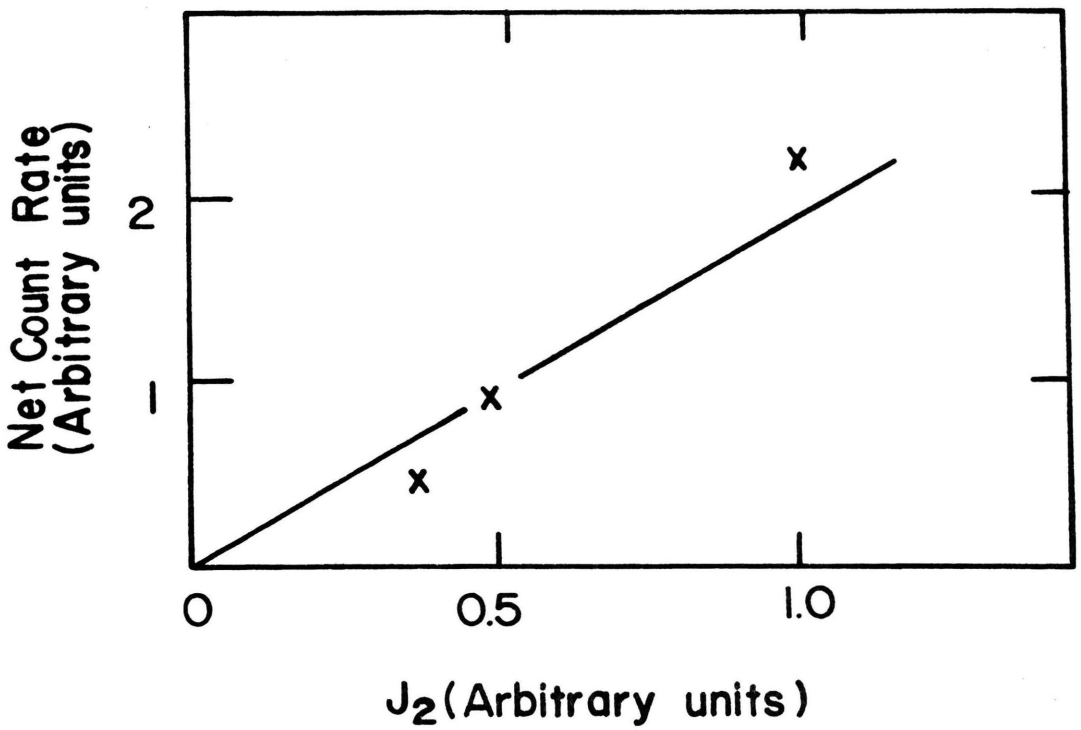

Fig. 12. Consistency check for the ionization radiation $j_2(\lambda)$. The dependence of the net count rate on the photon flux from the ionization radiation is shown. These measurements were taken at a constant atomic beam density and constant photon flux from the excitation radiation.

Since it is necessary to accumulate data for long periods of time at each point and since there are several points to be taken, it is necessary that $j_1(\lambda_o)$ and n_o be constant over this period. Also, $j_2(\lambda_2)$ must be constant over the observation times. Each of these were monitored for a period of 72 hours and it was observed that neither continually decreased nor increased. It was observed that $j_1(\lambda_o)$ and n_o did not fluctuate enough to be observable. Although there was some few per cent fluctuation in $j_2(\lambda)$, the average fluctuation approached zero in a short period of time.

C. Data and Discussion

From Eq. (1.4), the relative photoionization cross section, $\sigma_{rel}(\lambda)$, is given by

$$\sigma_{rel}(\lambda_2) = \frac{N^+(\lambda_2)}{j_2(\lambda_2)} \tag{5.6}$$

It should be pointed out again that the measurements were taken over a wavelength interval of the ionization radiation with a full-width, half-maximum spectral bandwidth of approximately 150 Å. Thus the observed count rates and photon flux are measured over this spectral band and the reported cross section will be an average cross section over that interval. This will have to be modified somewhat when interpreting the data in the "onset" region.

Data for the $6^2P_{3/2}$- and $6^2P_{1/2}$-states were taken at wavelengths corresponding to the intense spectral lines of the Hg-Xe ionization light source, 5460, 4358, 4047, 3663, 3130, and 2537 Å. The signal-to-noise ratio attainable for each of the above lines was approximately 1 to 100. For the remainder of the curve, data points in the continuum of the Hg-Xe lamp were taken with signal-to-noise ratios from 1 to 500 and 1 to 2000 for the $6^3P_{3/2}$- and $6^2P_{1/2}$-states, respectively. The different signal-to-noise ratio on this portion of the curve is due to the intensity difference (approximately 7) of the two exciting lines of the cesium discharge lamp. This effect was not as noticeable for wavelengths $\lesssim$ 4358 Å because of the high intensity of the ionization light source.

Data for wavelengths $\lesssim$ 4358 Å were taken over a total time period of approximately 3 hours per point. The remaining points represent a cumulative observation time of 10 hours. Even at these long counting times the statistical error for the upper portion of the curve is much larger than for the lower portion. To reduce this error to approximately the same as the other points, however, would require counting times of several hundred hours per point. This would require stability of the apparatus over a period of weeks and is not practical.

Once the two onsets are established, the error due to the spectral bandwidth can be eliminated. This is accomplished by observing the intensity distribution of the

ionization radiation, at a particular wavelength setting through a 1 meter Jarrell Ash monochromator. The fraction of the intensity below threshold is obtained from this distribution and corresponds approximately to the fraction of the photon flux, $j_2(\lambda_2)$, below threshold. This is then used in Eq. (1.5) to determine the cross section at that point.

Figs. 13a and 13b show the corrected data for the $6^2P_{3/2}$- and $6^2P_{1/2}$-states normalized to the theoretical curve of Weisheit[2]. The statistical error associated with these measurements are indicated by the error bars shown. As can be seen from each of the two curves, the present data decreases with decreasing wavelength more rapidly than predicted by theory.

Figs. 14a and 14b show the corrected data for the $6^2P_{3/2}$- and $6^2P_{1/2}$-states normalized to the experimental curve of Mohler and Boeckner[3]. Although Mohler and Boeckner's measurement was for the combined 6^2P-states, it is allowable to normalize the cross section for the fine structure levels to that of the combined states because each varies with wavelength in the same manner as the combined states[2,16]. Within statistical error the present results are in excellent agreement with that of Mohler and Boeckner.

Along with the statistical errors indicated in the various curves, it is possible to have a systematic error

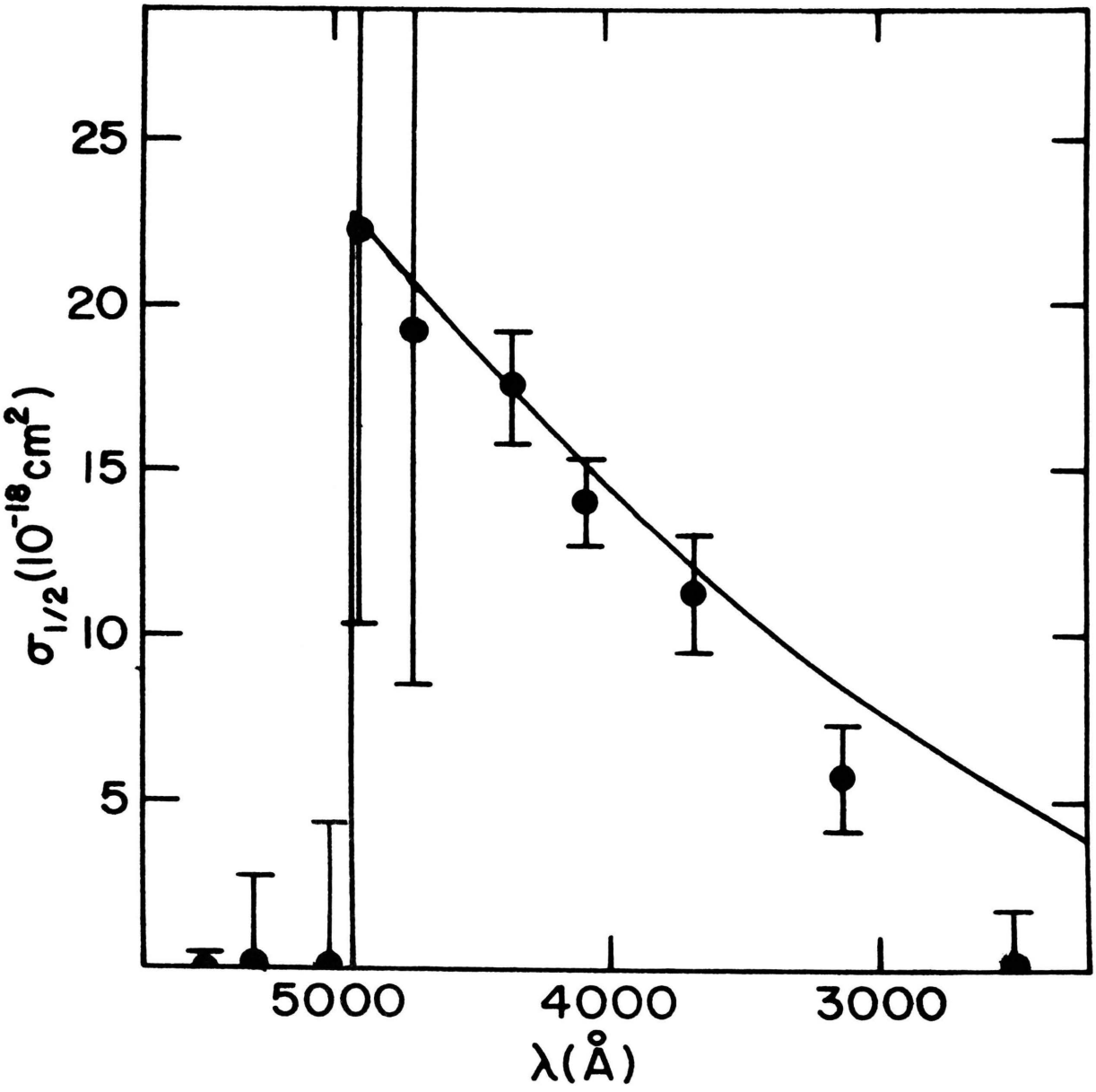

Fig. 13a. Photoionization cross sections for the $6^2P_{3/2}$-state of cesium. The curves are normalized to the theoretical curve of Weisheit[2] at 5000 Å and 4358 Å.

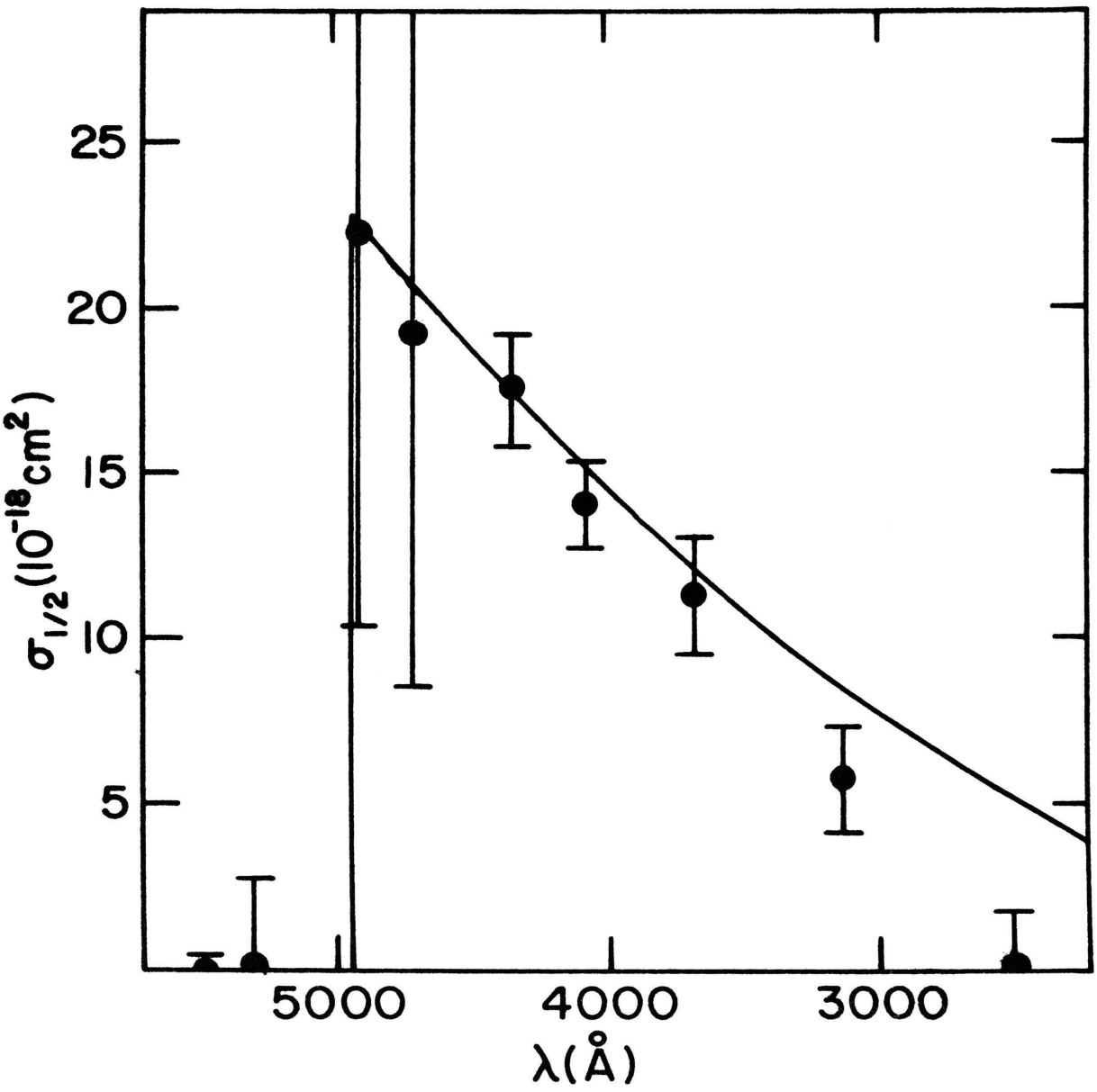

Fig. 13b. Photoionization cross sections for the $6^2P_{1/2}$-state of cesium. The curves are normalized to the theoretical curve of Weisheit[2] at 4900 Å and 4358 Å.

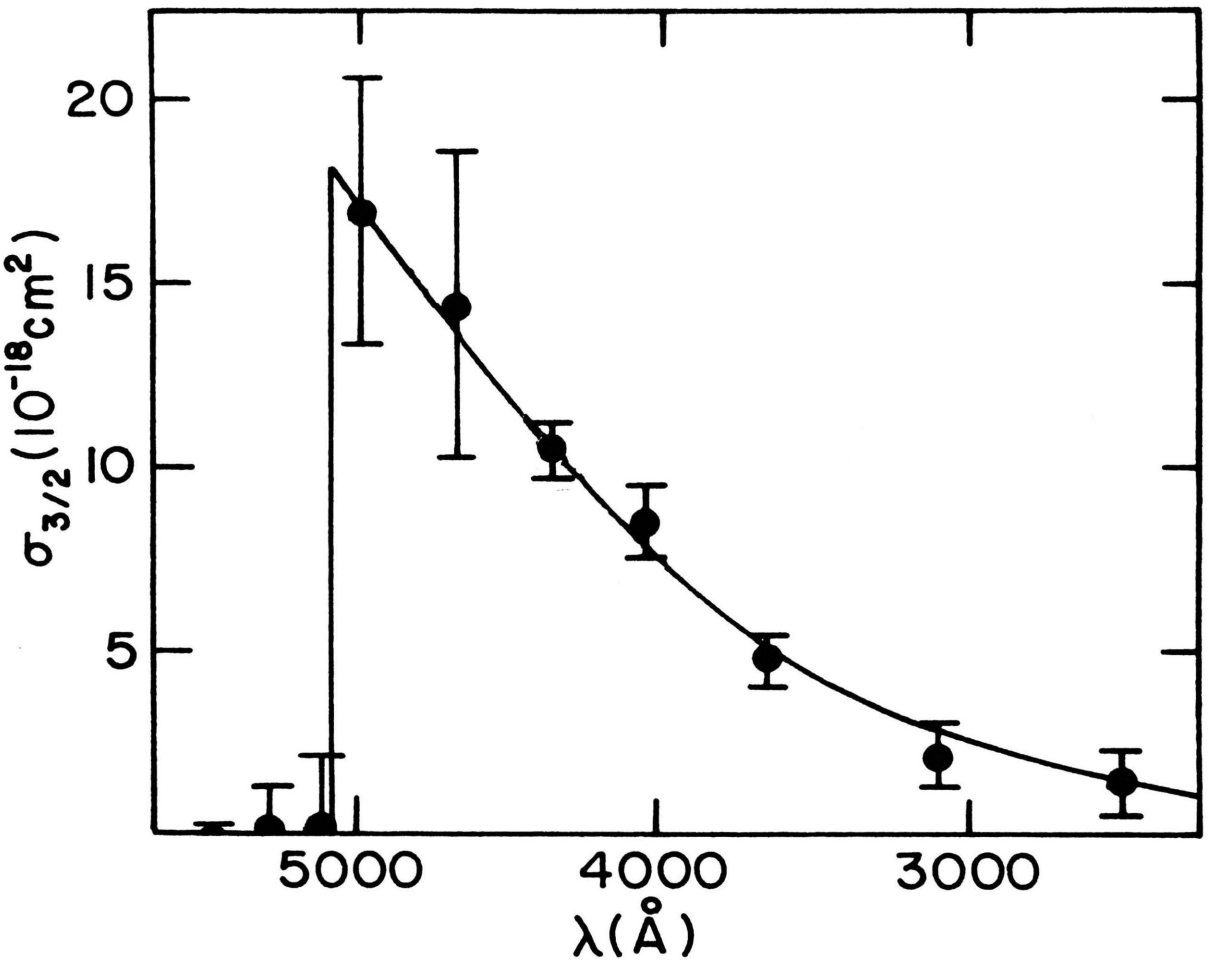

Fig. 14a. Photoionization cross sections for the $6^2P_{3/2}$-state of cesium. The curves are normalized to the experimental curve of Mohler and Boeckner[3] for the combined 6^2P-state at 5000 Å and 4358 Å.

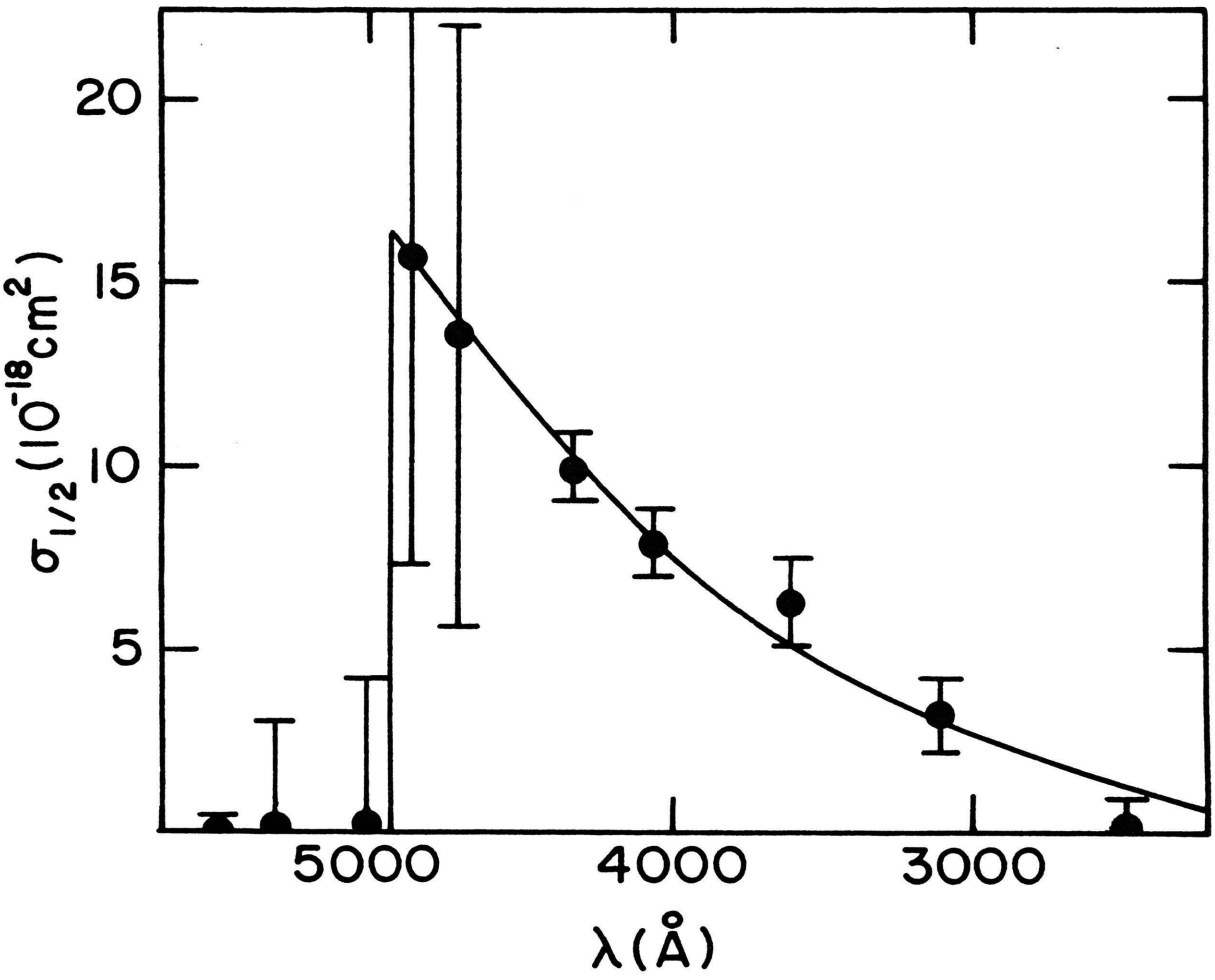

Fig. 14b. Photoionization cross sections for the $6^2P_{1/2}$-state of cesium. The curves are normalized to the experimental curve of Mohler and Boeckner[3] for the combined 6^2P-state at 4900 Å and 4358 Å.

of some few per cent due to the previously mentioned experimental errors. Allowing for these errors, however, the present results decrease more rapidly at short wavelength than predicted by theory.

BIBLIOGRAPHY

1. D.W. Norcross and P.M. Stone, J. Quant. Spectrosc. Radiat. Transfer 6, 277 (1966).
2. J.C. Weisheit, J. Quant. Spectrosc. Radiat. Transfer 12, 1241 (1972).
3. F.L. Mohler and C. Boeckner, Bur. Std. J. Res. 5, 51, (1930).
4. L. Agnew and C. Summers, Proc. VII Int. Conf. on Phenomena in Ionized Gases, Belgrade, 574 (1965).
5. E.W. McDaniel and M.R.C. McDowell, Case Studies in Atomic Collision Physics (John Wiley & Sons, Inc., New York, 1969), Vol. 1, pp. 49-71.
6. H.L. Davis, ed., Phys. Today 27, p. 17, 1974.
7. R.D. Hudson and L.J. Kieffer, Atomic Data 2, 205, (1971).
8. R.D. Hudson, Rev. Geophys. Space Phys. 9, 305 (1971).
9. H.J.J. Braddick and R.W. Ditchburn, Proc. Roy. Soc. (London) 143, 472 (1934).
10. R.F. Stebbings, F.B. Dunning, F.R. Tittel, and R.D. Rundel, Phys. Rev. Letters 30, 815 (1973).
11. G.V. Marr, Photoionization Processes in Gases, (Academic Press, Inc., New York, 1967), pp. 31-54.
12. H.A. Kramers, Phil. Mag. 46, 836 (1923).

13. T.C. Caves and A. Dalgarno, J. Quant. Spectrosc. Radiat. Transfer 12, 1539 (1972).

14. A. Burgess and M.J. Seaton, Mon. Not. Roy. Astron. Soc. 120, 121 (1959).

15. P.M. Stone, Phys. Rev. 127, 1151 (1962).

16. Yu. V. Moskvin, Optica and Spectroscopy 15, 316 (1963).

17. D.W. Norcross, private communication (1972).

18. M. Born and J.R. Oppenheimer, Ann. Phys. 84, 457 (1927).

19. G. Baum, M.S. Lubell, and W. Raith, Phys. Rev. Lett. 25, 267 (1970); K. Kessler and J. Lorenz, Phys. Rev. Lett. 24, 87 (1970).

20. The CHS was supplied by the Brunswick Corp., Skokie, Ill. 60076. The structure contained 5500 holes per in^2, each with a diameter-to-length ratio of 1:20.

21. N.F. Ramsey, Molecular Beams (Oxford, Clarendon Press, 1956), pp. 11-50.

22. M. Kaminsky, Atomic and Ionic Impact Phenomena on Metal Surfaces (Springer, Berlin, 1965), pp. 98-124.

23. H.A. Jones and I. Langmuir, Gen. Elec. Rev. 30, 310 (1927).

24. J.B. Taylor and I. Langmuir, Phys. Rev. 51, 753 (1937).

25. J.B. Taylor and I. Langmuir, Phys. Rev. 44, 423 (1933).

26. R.E. Hebner, Jr. and K.J. Nygaard, Physica 58, 225 (1972).

27. R.E. Hebner, Jr. and K.J. Nygaard, J. Opt. Soc. Am. 61, 1455 (1971).

28. Cesium Osram Spectral Lamp from the Edmund Scientific Company.

29. 250 Watt high pressure Hg-Xe vapor lamp and housing from Ushio Electronics, Tokyo, Japan.

30. Calibrated photodiodes from United Detector Technology, Inc., Santa Monica, California.

31. Johnson's Laboratories, Inc., Cockeysville, Maryland.

32. Model 1110 Digital Synchronous Computer from SSR Instruments Co., Santa Monica, California.

33. A.C.G. Mitchell and M.W. Zemansky, Radiation and Excited Atoms (The MacMillan Co., New York, 1934), pp. 92-151.

34. D.N. Creek and G.V. Marr, Proc. Roy. Soc. (London) A304, 233 (1968); D. Popescu, M.L. Pascu, C.B. Collins, B.W. Johnson, and Iovitzu Popescue, Phys. Rev. A 8, 1666 (1973).

35. R.H. McFarland and J.D. Kinney, Phys. Rev. A, 137, 1058 (1965).

36. H. Heil and B. Scott, Phys. Rev. A 145, 279 (1966).

37. Yu. P. Korchevoi and A.M. Przonski, Soviet Phys. - JETP 24, 1089 (1967).

38. K.J. Nygaard, J. Chem. Phys. 49, 1995 (1968).

39. F.L. Mohler and C. Boeckner, Bur. Standards J. Res. 3, 303 (1929).

40. E.O. Lawrence and N.E. Edlefsen, Phys. Rev. 34, 233 (1929).

41. M.J. Seaton, Proc. Roy. Soc. (London) 208A, 418 (1951).

42. J.C. Weisheit, private communication (1971).

43. K. Freudenberg. Z. Physik 67, 417 (1931).

44. D.H. Pollock and A.O. Jensen, J. Appl. Phys. 36, 3184 (1965).

45. A.G.F. Kniazzeh, Report on the Twenty-Sixth Annual Conference on Physical Electronics (MIT, Cambridge, Massachusetts, 1966), p. 1.

46. O.P. Breaux and G. Medicus, Phys. Rev. Letters 16, 392 (1966).

47. M.L. Shaw and R.E. Stickney, Phys. Rev. Letters 18, 824 (1967).

48. W.J. Price, Nuclear Radiation Detection (McGraw-Hill Book Co., New York, 1964), 2nd ed., pp. 52-69.

VITA

John Daniel Jones was born on February 10, 1948 in Dahlonega, Georgia. He received his primary and secondary education in Dahlonega. He has received a Bachelor of Science degree in physics from North Georgia College in 1969 and a Master of Science degree in physics from the University of Missouri-Rolla in 1971.

While working on his Doctor of Philosophy, he was a teaching assistant and a research assistant with support from the Office of Naval Research.